A Numerical Study of Dynamic Responses of Two Selected Flexible Rockfall Barriers Subject to Punching and Areal Loads

GEO Report No. 323

R.C.H. Koo & J.S.H. Kwan

Geotechnical Engineering Office
Civil Engineering and Development Department
The Government of the Hong Kong
Special Administrative Region

A Numerical Study of Dynamic Responses of Two Selected Flexible Rockfall Barriers Subject to Punching and Areal Loads

GEO Report No. 323

R.C.H. Koo & J.S.H. Kwan

Preface

In keeping with our policy of releasing information which may be of general interest to the geotechnical profession and the public, we make available selected internal reports in a series of publications termed the GEO Report series. The GEO Reports can be downloaded from the website of the Civil Engineering and Development Department (http://www.cedd.gov.hk) on the Internet. Printed copies are also available for some GEO Reports. For printed copies, a charge is made to cover the cost of printing.

The Geotechnical Engineering Office also produces documents specifically for publication in print. These include guidance documents and results of comprehensive reviews. They can also be downloaded from the above website.

These publications and the printed GEO Reports may be obtained from the Government's Information Services Department. Information on how to purchase these documents is given on the second last page of this report.
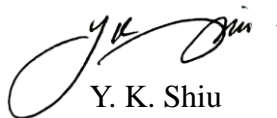
H.N. Wong
Head, Geotechnical Engineering Office
November 2016

Foreword

This report presents results of a numerical study on the performance of two selected flexible rockfall barriers subject to punching load and areal load using non-linear finite element numerical package LS-DYNA. The punching load and areal load simulate rockfall impact and landslide debris impact respectively. Numerical structural models of flexible barriers developed by Arup and AECOM were modified to simulate the impact loads in this study.

This study was carried out by Mr R.C.H. Koo and Dr J.S.H. Kwan under my supervision. Mr T.H. Lo assisted in the numerical analyses. Contributions from all parties are gratefully acknowledged.

Y. K. Shiu
Chief Geotechnical Engineer/Standards & Testing

Abstract

A numerical study on the performance of two selected flexible rockfall barriers subject to punching and areal loads was undertaken. The punching and areal loads simulate rockfall impact and landslide debris impact respectively. Numerical simulations were carried out using three-dimensional non-linear finite element numerical package LS-DYNA. In the numerical simulations, the two flexible barriers were impacted by drop weights moving at different velocities. Drop weights of different shapes such as single sphere and rigid-slab were used. The impacts of the sphere and the rigid-sphere are pertinent to punching load and areal load scenarios respectively.

The numerical analyses show that the two rockfall barrier structures could withstand the impact of the rigid-slab with the kinetic energy same as their energy capacity, and that the impacts of rigid-slab could give rise to a higher foundation load in the direction of the impact when compared with the punching load.

Contents

List of Tables

List of Figures

1 Introduction

Proprietary rockfall barriers to mitigate rockfall hazards are available from many suppliers. Rockfall barriers are rated by impact energy that a set of panels can absorb without being breached. Their performance in catching rockfall is usually verified by full-scale tests and certified against various national or European standards (e.g. EOTA, 2008). Flexible rockfall barriers have occasionally been impacted by landslide debris in different places including Hong Kong (Kwan & Koo, 2013). A number of field cases have demonstrated that flexible rockfall barriers could be capable of arresting a certain amount of landslide debris (Duffy, 1998; Roth et al, 2004; Wendeler et al, 2006). However, knowledge on the performance of flexible rockfall barriers subjected to impact of landside debris is still limited to date.

The loading patterns between the impacts of rockfall and those of landslide debris are different, and hence different dynamic responses of flexible rockfall barriers. For example, rockfall produces punching load acting on a relatively small area in a momentarily instant, but landslide debris would act over a larger area for a longer period of time.

Large-scale physical tests of flexible barriers impacted by landslide debris were undertaken by WSL (2010). In the tests, 'landslide debris' was simulated by releasing mixtures of water and soils and rocks at crest of a slope, and a flexible barrier was installed at the toe of the slope. Although the test results provide useful field data on the performance of the barrier, large-scale tests of this kind are fraught with problems including repeatability and little control of the impact velocity and density of debris.

Advanced numerical tools nowadays can provide useful means of analyzing the behavior of flexible structures. For examples, Tang et al (2009) and Volkwein (2004) used numerical simulations to analyze and gain better understanding of the performance of flexible barriers in rockfall tests.

In this study, the computer program LS-DYNA is used to simulate flexible rockfall barriers subjected to punching and areal loads with a view to examining and comparing the performance of the barriers in resisting rockfall and impact of landslide debris respectively. Structural details of the flexible rockfall barriers considered in this study are the same as those reported by Volkwein (2004) and Maccaferri (2011).

2 Literature Review

2.1 Responses of Flexible Barriers Subject to Rockfall and Landslide Debris Impacts

A flexible barrier system consists of steel posts fixed in position by uphill and/or lateral steel ropes and post foundations. Netting, which may comprise a series of rings made of 3 to 5 mm spiralled steel wires, is draped along cable ropes spanning across the posts. The netting is free to slide along the cable ropes when it is subject to impact. The sliding of netting plays an important role in load transfer within the flexible barrier structure, as it changes the profile, elongation and inclination of cable ropes. In general, shackles carrying the barrier netting slide towards the middle portion of a cable upon impact by a rockfall (see Figure 2.1).

Figure 2.1   Shackles Carrying the Barrier Net Move towards the Middle of Cable after Rockfall Impact (Volkwein, 2004)

Geobrugg and WSL carried out field tests of flexible barriers impacted by debris flows and landslide debris as well as full-scale rockfall tests (Geobrugg, 2007 & 2010; WSL, 2009 & 2010).   Wendeler (2013) consolidated the field observations and experience gained in the tests and discussed the effects of rockfall impact and landslide debris impact on various components of the flexible barriers.   She opined that the rope cable components of the barriers subjected to rockfall and landslide debris impacts would not be critical, as energy dissipation devices control the development of cable force.   For ring nets, landslide debris impact could represent a less structurally demanding scenario because the landslide debris has a larger loading area comparing with rockfall.   She indicated that landslide debris impact could result in higher anchor or foundation loads than rockfall impact.

Margreth & Roth (2008) reported that some flexible rockfall barriers had been damaged by snow avalanches in Austria.   Impact load patterns induced by snow avalanches and landslide debris could be similar, and hence could be relevant to this study.   Margreth & Roth (op cit) summarised their observations on the damaged flexible rockfall barriers over four winters from 2003 to 2006.   They noted that barrier post foundations could be vulnerable to damage when the barriers were subject to impact by snow avalanche, and recommended that post foundation should be properly reinforced and post spacing reduced.

2.2   Computer Programs for Analyzing Flexible Barriers

In early 2000s, Nicot et al (2001) adopted an explicit numerical algorithm to develop a computer program to simulate flexible barriers.   Special attention was paid to the modelling of the structural behaviour of ring nets.   The program modelled ring net as a hexagonal mesh. The structural properties of the mesh were calibrated based on results of load tests on ring nets.   The performance of the program was tested against a full-scale experiment of a falling rock block impacting on a flexible barrier.   However, the actual mechanism of the rings moving along the rope cable was not considered.

Another computer program developed in Europe to simulate rockfall barriers is FARO

(Volkwein, 2004).   The program adopts a spring model whereby the stiffness of a ring in the ring net is modeled by a pair of diagonal spring elements in a four-sided ring.   A non-linear finite-element numerical procedure is used.   FARO has been calibrated against rockfall tests but the connection between ring net and rope cable is not explicitly modelled.   Details of the test set-up can be found in Volkwein (2004) and Grassl (2002).

Chan et al (2012) also developed a computer program capable of analysing flexible barriers.   The program was developed by modifying a non-linear finite-element structural package, NIDA.   Special 'sliding cable element' has been built into NIDA to simulate the sliding of the netting along cable ropes.   To realistically capture the behaviour of the netting, frictional forces between the contact points of the nets are considered in the calculations. This program has been verified against the published results of debris flow field tests in Switzerland by Geobrugg (Zhou et al, 2011).   However, this program can only conduct pseudo-static analysis.

Tang et al (2009) reported the use of finite element software package, LS-DYNA, to model flexible rockfall barriers.   LS-DYNA is a versatile structural package, originally developed for simulations of dynamic process involving large deformations e.g. car crash. More recently, GEO has commissioned Arup to undertake numerical studies of the performance of flexible barriers impacted by debris flows.   Fully coupled analyses involving debris mobility and structural response were carried out.   As part of the Arup's studies, the rockfall tests carried out by Volkwein (2004) were repeated numerically.   The rockfall barrier put to the test was installed horizontally in a test rig.   The results are in good agreement with the test data (Arup, 2013).

3   Study Scope

In this Technical Note, three numerical studies on the performance of simulated flexible rockfall structures are presented.   Rockfall and landslide debris impacts are simulated by punching and areal loads respectively.   Numerical simulations are carried out using three-dimensional non-linear finite element numerical package LS-DYNA.   A summary of each numerical study and its primary objective are presented below:

(a) The behavior of horizontal flexible rockfall net simulated by Arup (2013) is validated against the experimental results of the rockfall test reported by Volkwein (2004).   This is used to demonstrate that the program LS-DYNA is an appropriate tool for the analysis of flexible rockfall structures.

(b) After the validation of the LS-DYNA model, a series of numerical simulations is carried out to compare the performance of the Volkwein's net subject to impact of punching and areal loads.

(c) In addition, the vertical flexible rockfall barrier simulated by Ng et al (2012) is adopted to repeat the impact of punching and areal loads to the vertical barrier.

4   Numerical Simulation of the Rockfall Test of Volkwein (2004)

The aim of the captioned study is to check the validity of the numerical model developed by Arup (2013) in simulating the responses of flexible rockfall structures subjected to a punching load, by simulating the physical rockfall tests undertaken by Volkwein (2004). The Swiss Institute for Snow and Avalanche Research, the Institute for Structural Engineering and Construction of the Swiss Technical College Zurich and Geobrugg provided technical and financial support to carry out the physical tests.

The rockfall tests were carried out in early 2000s.   The test rig is shown in Figure 4.1. The dimension of the panel of flexible barrier in the test was 3.7 m by 3.7 m.   The ring net was supported horizontally by four cables.   The energy rating of the barrier is 550 kJ.   The barrier was impacted by a spherical weight of 0.82 m diameter, dropped vertically from different heights.   The mass of the weight is 825 kg.   Tests were conducted with and without brake elements to investigate the performance of the flexible barrier.   Dimensions and engineering properties of all components of the barrier together with the test results were documented by Grassl (2002) and Volkwein (2004) in detail.

Figure 4.2 presents the numerical model set-up in LS-DYNA.   The steel frame of the test rig is not shown for clarity.   Ring net is explicitly modelled numerically by specifying the size and the engineering properties of the wires which made up the ring.   Figure 4.3 shows the simulation results of the rockfall test in which the weight was dropped from 16 m. Comparisons between the calculated and the measured displacements are given in Figure 4.4. A full account of the LS-DYNA simulations of the rockfall tests is given in Appendix A. The LS-DYNA analysis successfully reproduces the rockfall tests and the simulated results match reasonably well with the measured data.   This has validated that the numerical model developed by Arup (2013) can be used to study the behaviour and performance of the flexible rockfall barriers subject to impact loads.

Test Rig   Plan View
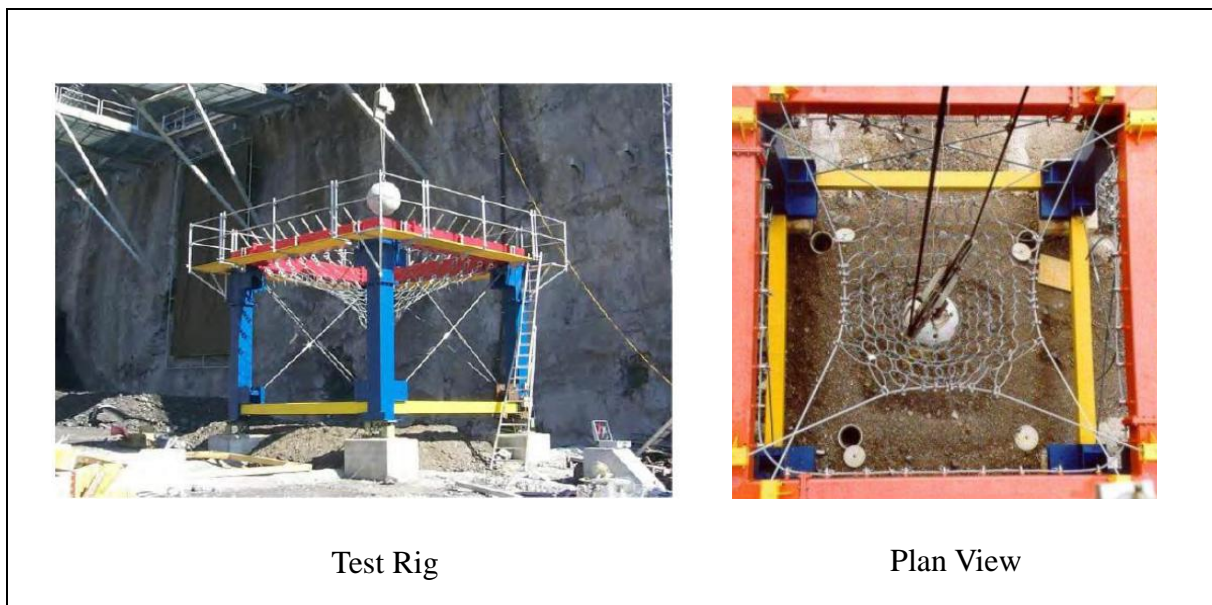
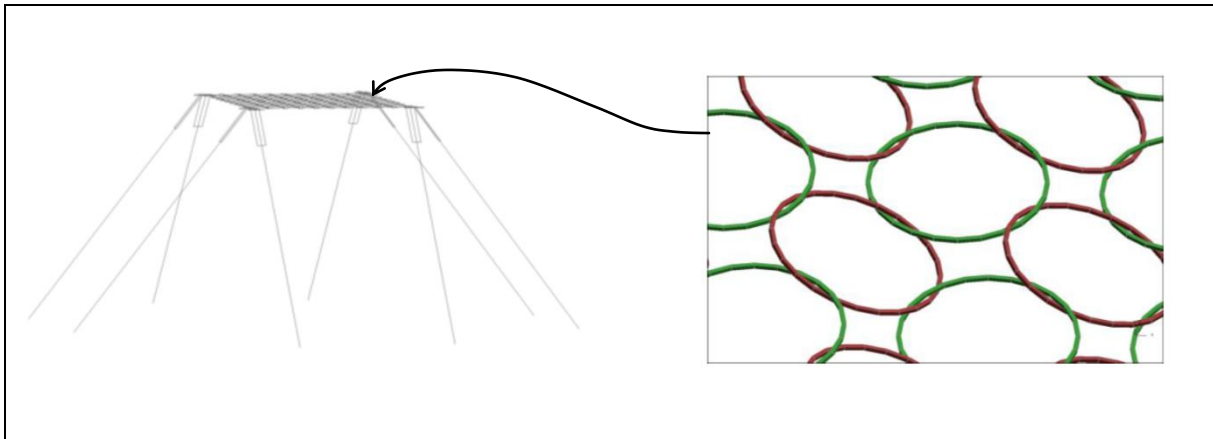**Figure 4.1   The Specifically-built Test Rig for Rockfall Tests (Volkwein, 2004)**

Figure 4.2 (Left) Structural Model Set-up in LS-DYNA (Steel Frame of the Test Rig not Shown for Clarity); (Right) Close-up of the Ring Net Model (Arup, 2013)
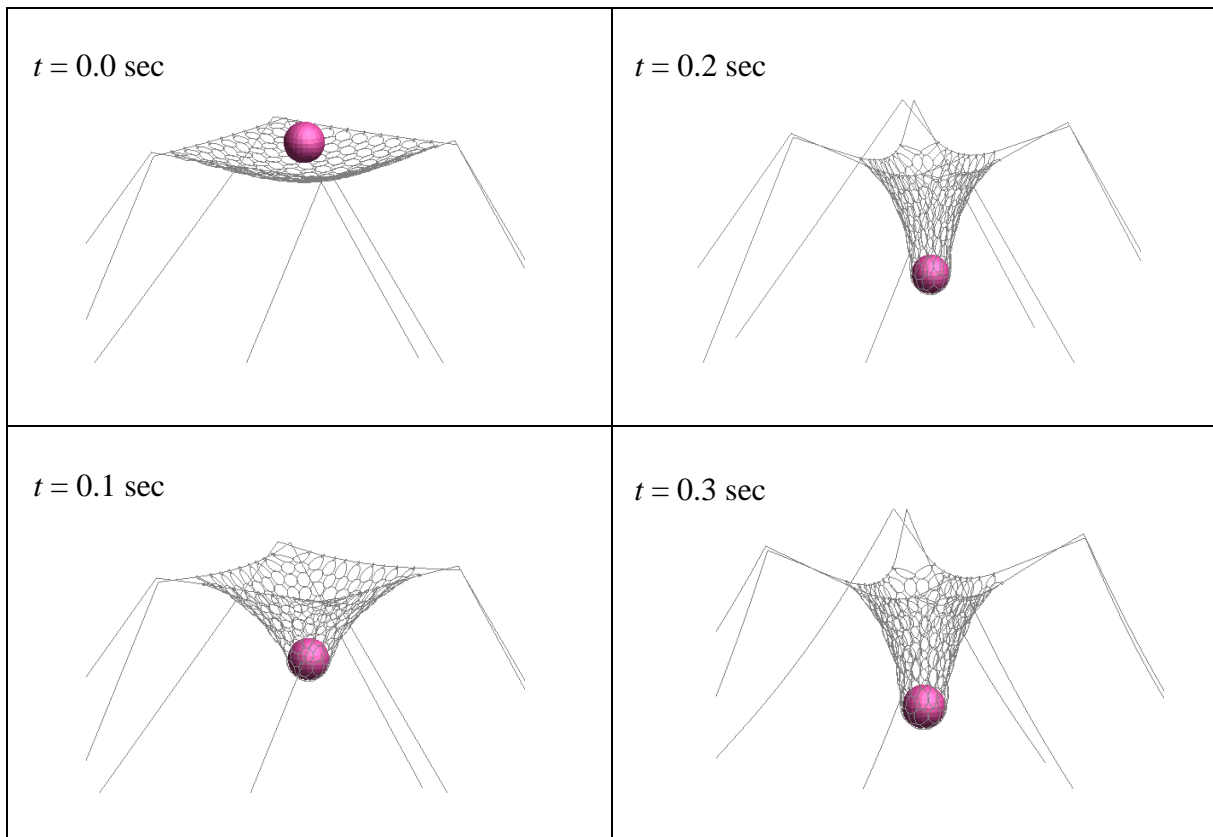

$t = 0.0$ sec

$t = 0.2$ sec

$t = 0.1$ sec

$t = 0.3$ sec

Figure 4.3 Simulation of Rockfall Tests of 16 m Drop Height

Note: Displacement = 0.0 m when the weight is in contact with the flexible barrier.
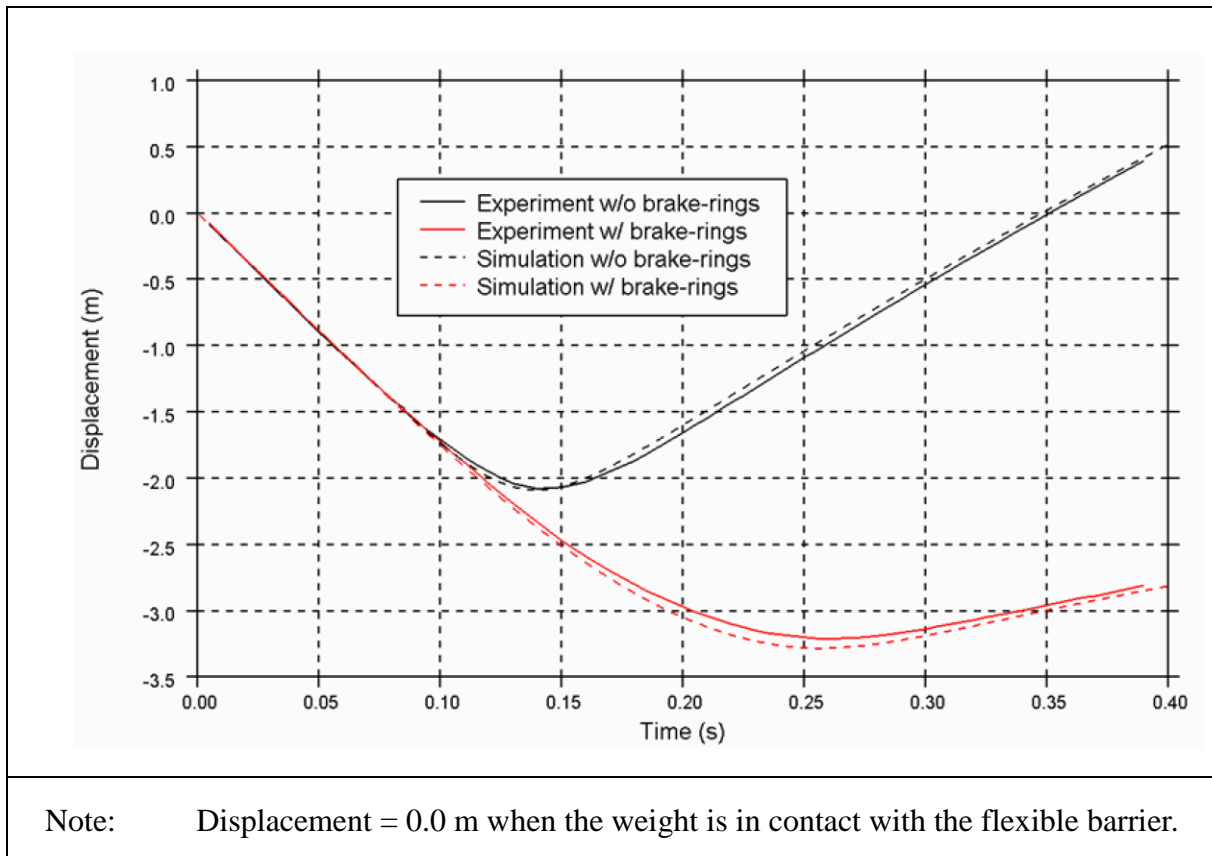
Figure 4.4   Simulated and Measured Displacements of the Drop Weight in Rockfall Tests

5   Numerical Study of Response of a Horizontal Net Subject to Punching and Areal Loads

A series of numerical simulations has been carried out using the verified LS-DYNA model, developed by Arup (2013), to study the performance of the horizontal flexible rockfall net subject to punching and areal loads.   Drop weights of different shapes were used in the simulations to create different load patterns.   They include (i) single-sphere, (ii) four-sphere, and (iii) rigid-slab (see Figure 5.1).   The single-sphere drop weight has a diameter of 0.82 m. It was used to simulate a punching load.   The rigid-slab, measuring 3 m by 3 m on plan, is made up of 25 spheres (5 on each side) with the same diameter of 0.6 m and connected together using fixed joints.   The loaded area created by this rigid-slab covers about 70% of the flexible barrier panel.   For comparison purposes, numerical tests using four-sphere drop weight were also conducted.   This four-sphere is made up of four unconnected spheres. The diameter of the sphere is 0.82 m.   The four spheres are in contact with each others. The corresponding loaded area of the four-sphere drop weight is about 1.6 m by 1.6 m.   The spheres were modelled using rigid shell elements.   The shell thickness was chosen such that all the drop weights have the same mass of 825 kg.

The drop weights were set to impact on to the barrier from different heights, hence at different kinetic energy levels from 90 kJ to 560 kJ.   The corresponding velocities are in the range of 14.9 m/s to 36.6 m/s.   Table 5.1 summaries the simulation schedule.
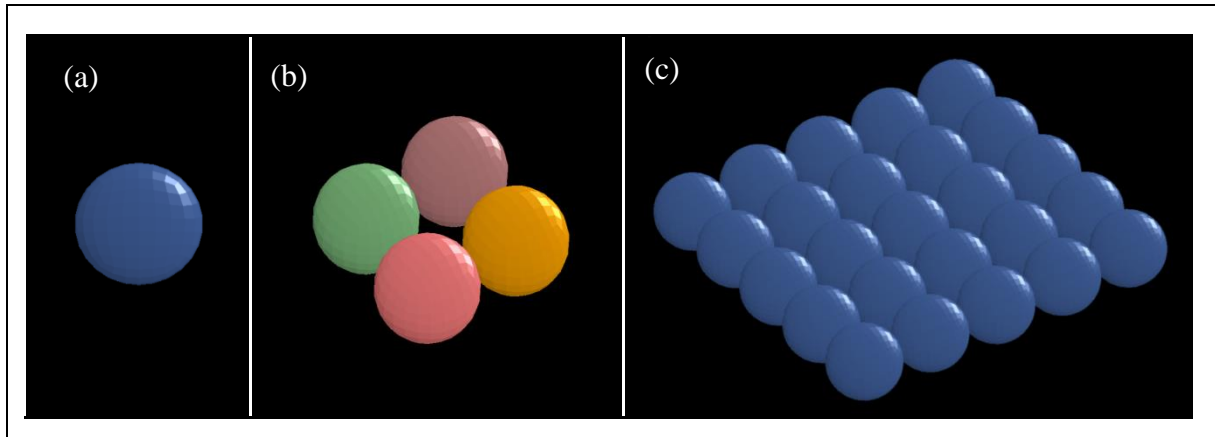
Figure 5.1   Drop Weights (a) Single-sphere, (b) Four-sphere, and (c) Rigid-slab

Table 5.1   Simulation Schedule for Study of Horizontal Net

Simulation No.	Drop Weight	Dimension	Contact Area	Impact Velocity (m/s)	Kinetic Energy (kJ)
1	Single-sphere	0.82 m dia.	5% of the barrier panel	14.9	90
2				18.6	143
3				22.7	215
4				27.2	309
5				31.9	425
6				36.6	559
7	Four-sphere	Each sphere: 0.82 m dia.	20% of the barrier panel	14.9	90
8				18.6	143
9				22.7	215
10				27.2	309
11				31.9	425
12				36.6	559
13	Rigid-slab	Each sphere: 0.6 m dia. Slab: 3 m by 3 m	70% of the barrier panel	14.9	90
14				18.6	143
15				22.7	215
16				27.2	309
17				31.9	425
18				36.6	559

5.1   Simulation Results

Figure 5.2 shows the graphical outputs of simulation nos. 3, 9 and 15.   It depicts the deformed barrier from the instant when the drop weights touched the barrier until the maximum deformation was reached.

The barrier system provides resistance against the impact of the drop weights.   The vertical acceleration and displacement time histories of simulation no. 3 for a single sphere are presented in Figure 5.3.   The model simulated free fall of the drop weight.   Before the drop weight was intercepted by the barrier, the vertical acceleration (a) of the drop weight was -9.81 m/s^2 (negative denotes downward direction).   When the drop weight reached the barrier (time, t = 0.0 second), the barrier provided an upward force to the drop weight, and the acceleration changed from downward to upward with a very short time.   The downward displacement of the drop weight continued until the drop weight was momentarily stopped. At that moment, the drop weight experienced the largest upward force (i.e. the largest a). Afterwards, the drop weight rebounded upwards and left the barrier, when a reverts back to -9.81 m/s^2.   According to the LS-DYNA simulations, the whole process lasted for about 0.3 second.

Figure 5.4 shows the vertical acceleration time histories for simulation nos. 3, 9 and 15. The maximum acceleration of the rigid-slab is the highest amongst the drop weights.   The time for stopping the rigid-slab is the shortest comparing with the others.   As shown in Figure 5.2, the time required to stop the rigid-slab is 0.12 second; while the four-sphere and the single-sphere were stopped by the barrier in 0.18 second and 0.21 second respectively.

The upward force provided by the barrier to the drop weight can be calculated based on the accelerations of the drop weights.   Figure 5.5 shows the maximum upward forces experienced by the drop weights in different numerical simulations.   With the 'action-and-reaction' principle, the upward forces would be equal to the vertical reactions at the foundation of the test rig.   It is assumed that the energy loss due to friction between the movable components of the barrier is substantially lower than the impact energy involved. The results infer that foundation load increases with the kinetic energy (or the impact velocity) of the drop weight.

The data in Figure 5.5 also shows that the rigid-slab resulted in higher foundation load comparing with the other drop weights.   The single-sphere drop weight induced the smallest foundation load.   The difference in the calculated foundation load produced by the rigid-slab and the single-sphere is 36% on average.

The LS-DYNA results show that landslide debris impact may induce a higher barrier foundation load compared with that induced by rockfall impact for identical kinetic energy levels of the impacts.   This finding appears to be consistent with the field observations by Margreth & Roth (2008) and Wendeler (2013) (see also Section 2.1).
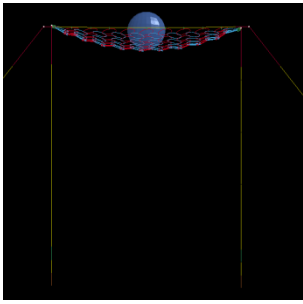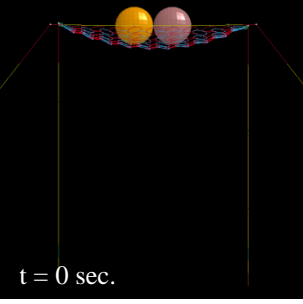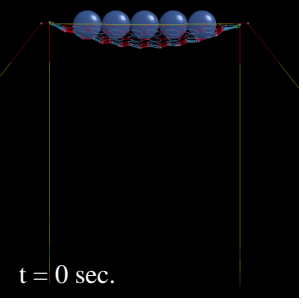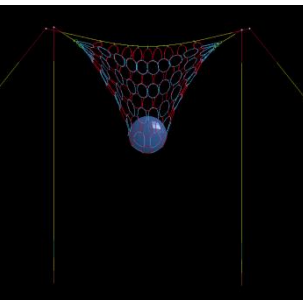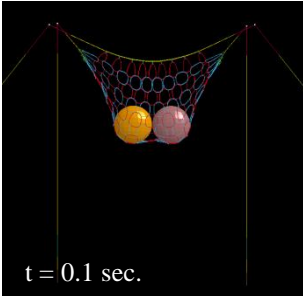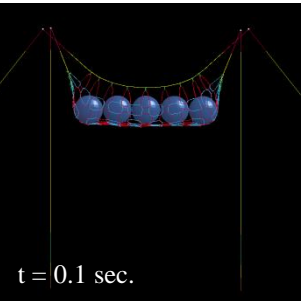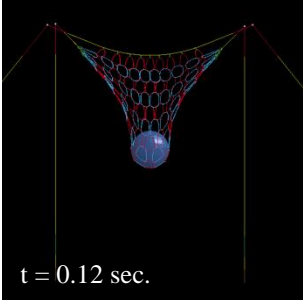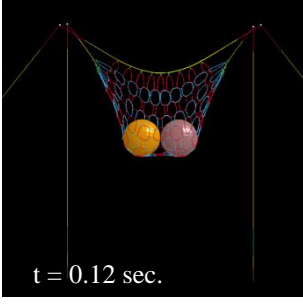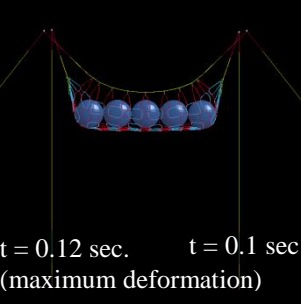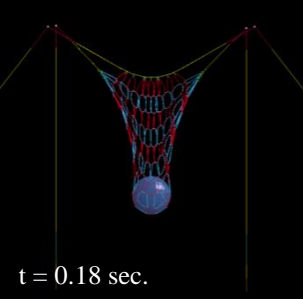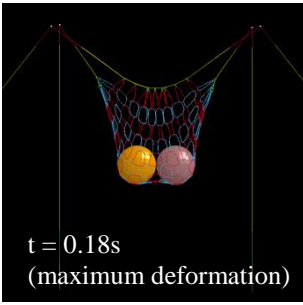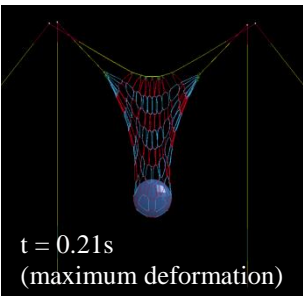
Simulation No. 3	Simulation No. 9	Simulation No. 15
	t = 0 sec.	t = 0 sec.
	t = 0.1 sec.	t = 0.1 sec.
t = 0.12 sec.	t = 0.12 sec.	t = 0.12 sec. t = 0.1 sec (maximum deformation)
t = 0.18 sec.	t = 0.18s (maximum deformation)	---
t = 0.21s (maximum deformation)	---	---

Figure 5.2   Graphical Outputs of Simulation Nos. 3, 9 and 15
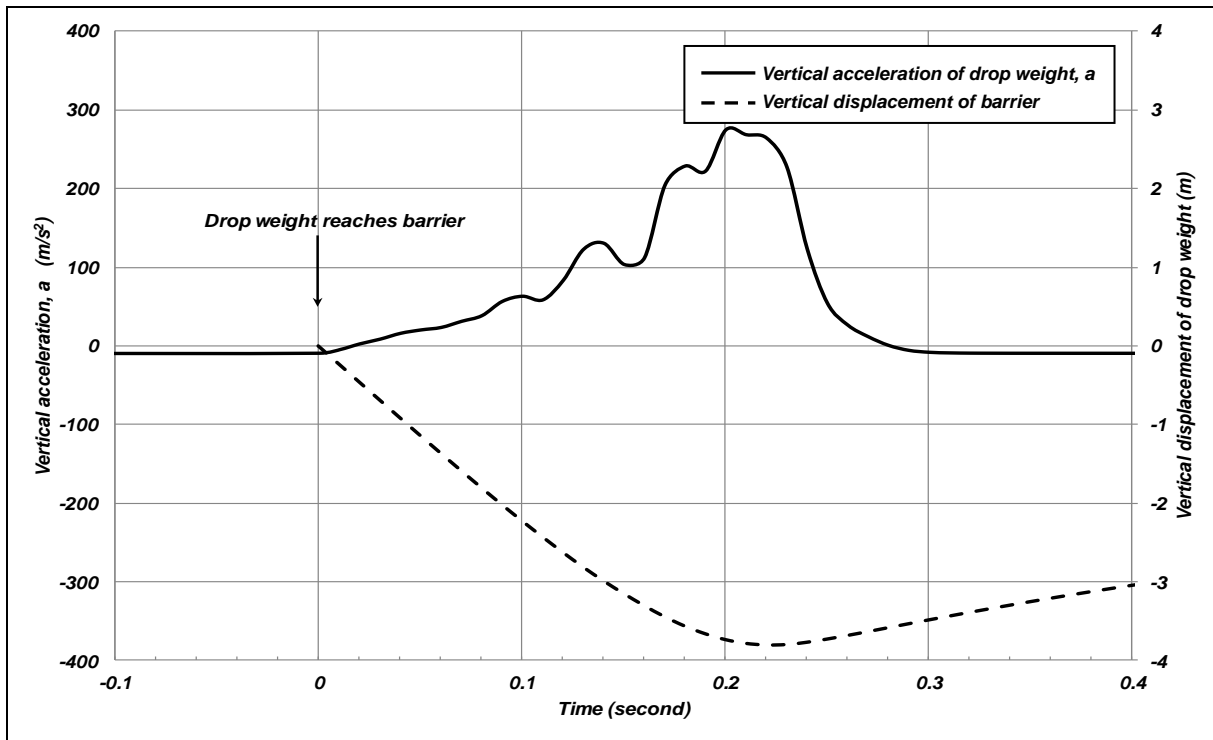
Figure 5.3   Vertical Acceleration and Displacement of the Drop Weight in Simulation No. 3
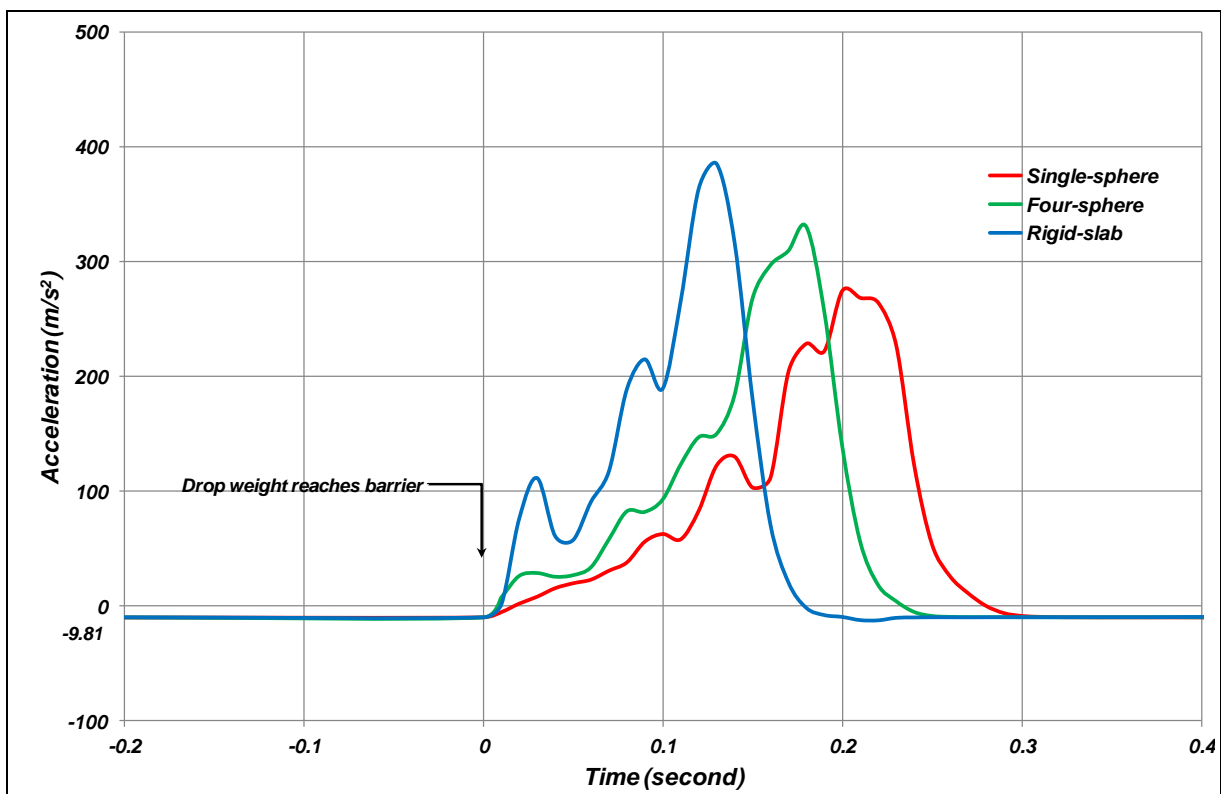
Figure 5.4   Vertical Acceleration of Drop Weight in Simulation No. 3, 9 and 15 (Sign Convention: Positive is Upward, Negative is Downward)
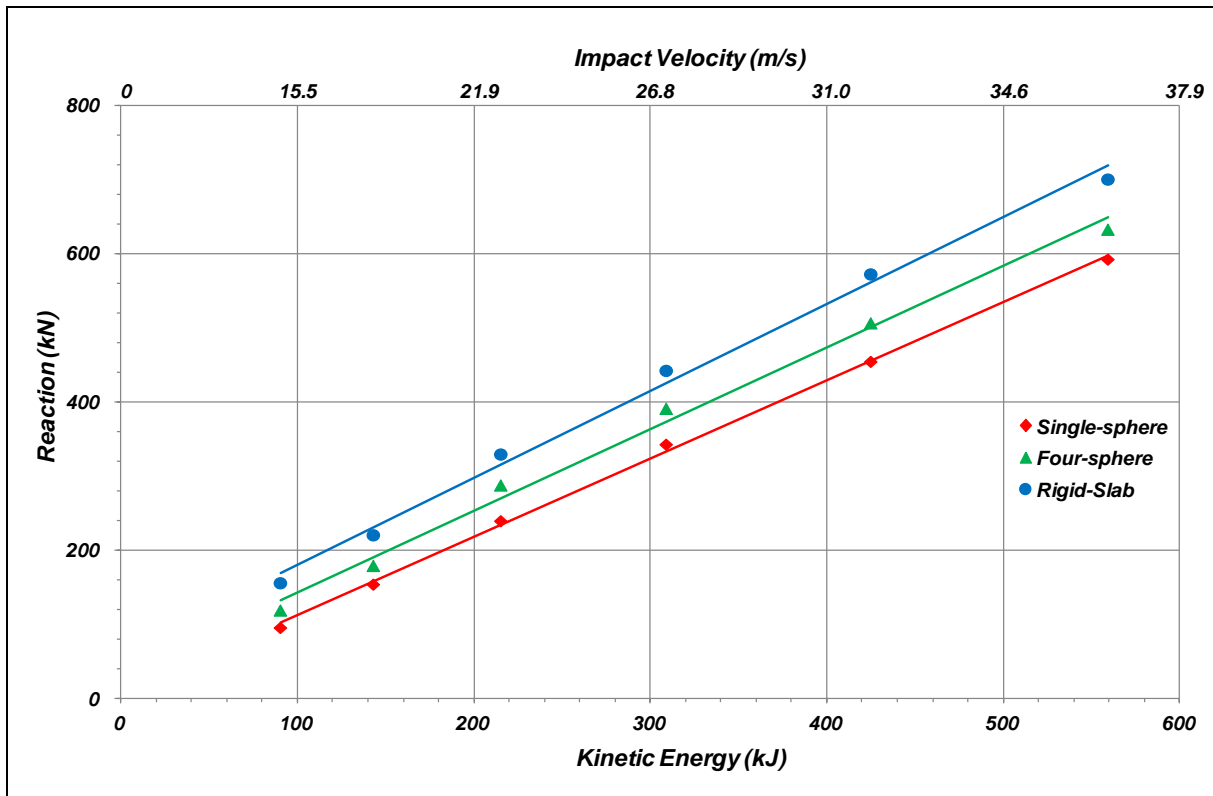
Figure 5.5   Reaction of Horizontal Net against Impact Velocity and Kinetic Energy

5.2   Cable Force

Figure 5.6 shows the cable forces calculated in the simulations.   There is no notable difference in cable forces produced by impacts of different drop weights.   Wendeler (2013) suggested that the cable force induced by rockfall and landslide impact of the same energy level could be similar if cables are equipped with energy dissipating device.   It is because that the forces mobilized in the cables are controlled by the load-deformation characteristics of the energy dissipating device.

The barrier net is supported by four cables in the flexible barrier (see Figure A1 in Appendix A).   The upward force experienced by the drop weights pertains to the vertical component of the cable force.   Figures 5.7(a) and 5.7(b) present graphical outputs of simulation nos. 3 and 15 at the time when the barrier deformation is the largest.   The inclination of the cable to the horizontal is denoted by θ.   The vertical component of the cable force is the product of cable force and $\sin\theta$.   Figure 5.8 shows the maximum values of θ recorded in different simulations.   It is noted that for a given impact energy level, the value of θ of single-sphere impact is the least, and that of rigid-slab impact is the largest.   The inclination of cable is controlled by the geometry of the deformed barrier net after the impact. Single-sphere impacts would result in localised barrier net deformations (see Figure 5.7(a)). The netting slides towards and is draped mainly by the middle portion of the cables. Photograph of the physical drop test of flexible barrier is also included in Figures 5.7(c).   In contrast, rigid-slab, which covers a relatively large area of the netting, restrains the movement of netting along the cables.   The netting is draped over a larger portion of the cables (c.f. Figure 5.7(b)) and thus giving rise to a larger cable inclination.
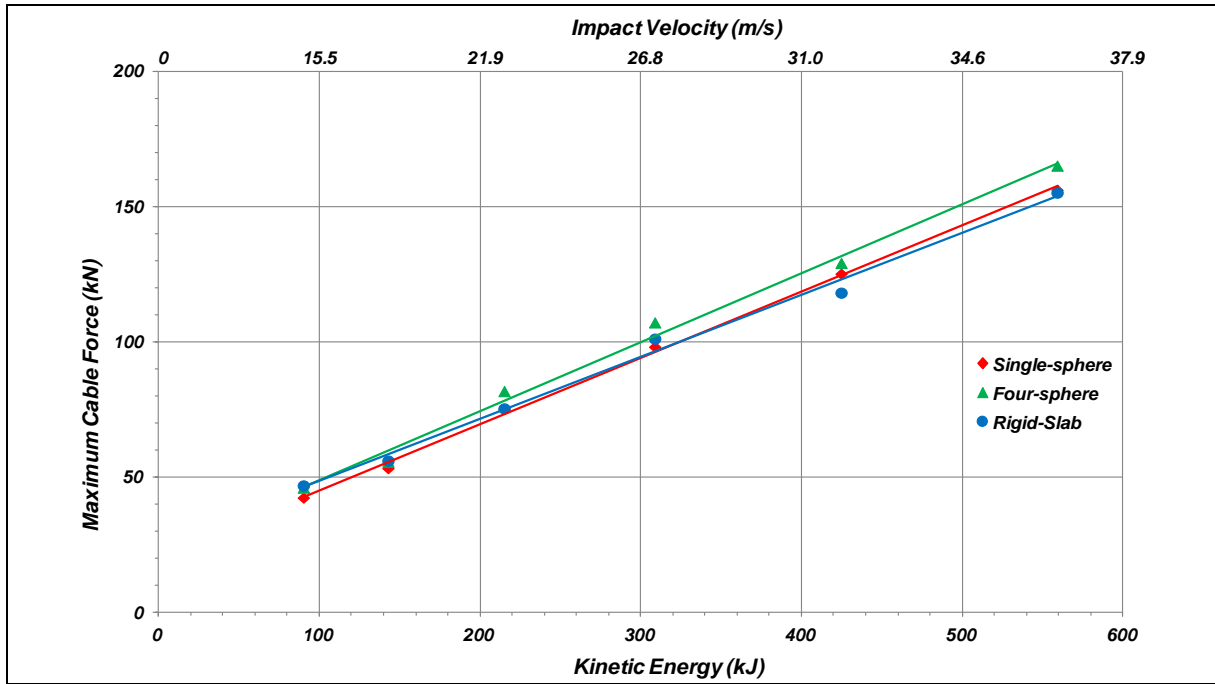
Figure 5.6   Cable Force against Impact Kinetic Energy

(a) LS-DYNA graphical output
(single-sphere)

(b) LS-DYNA graphical output
(rigid-slab)

(c) Vertical rockfall test
(Geobrugg, 2009)
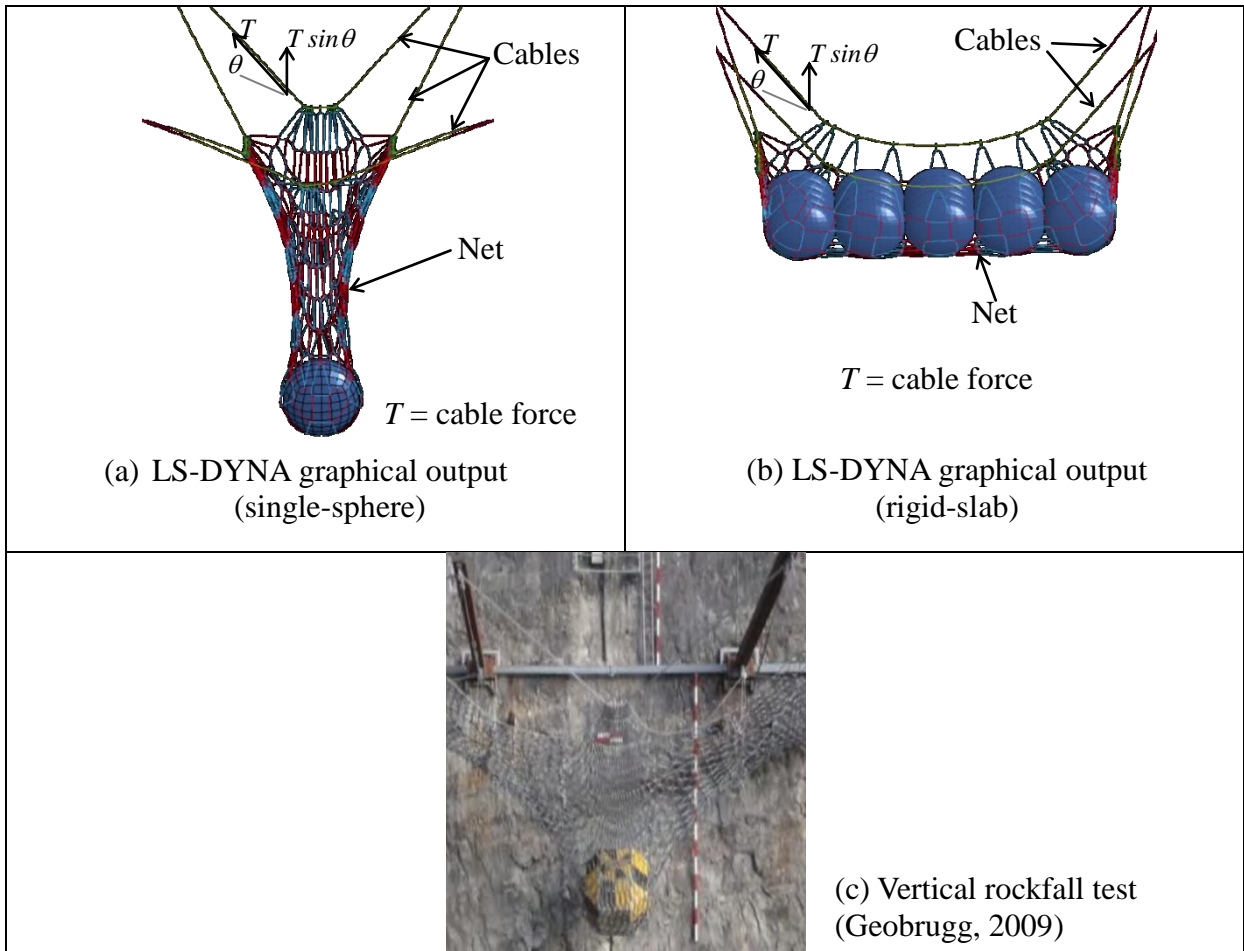
Figure 5.7   Geometry of Deformed Barriers under Different Load Patterns
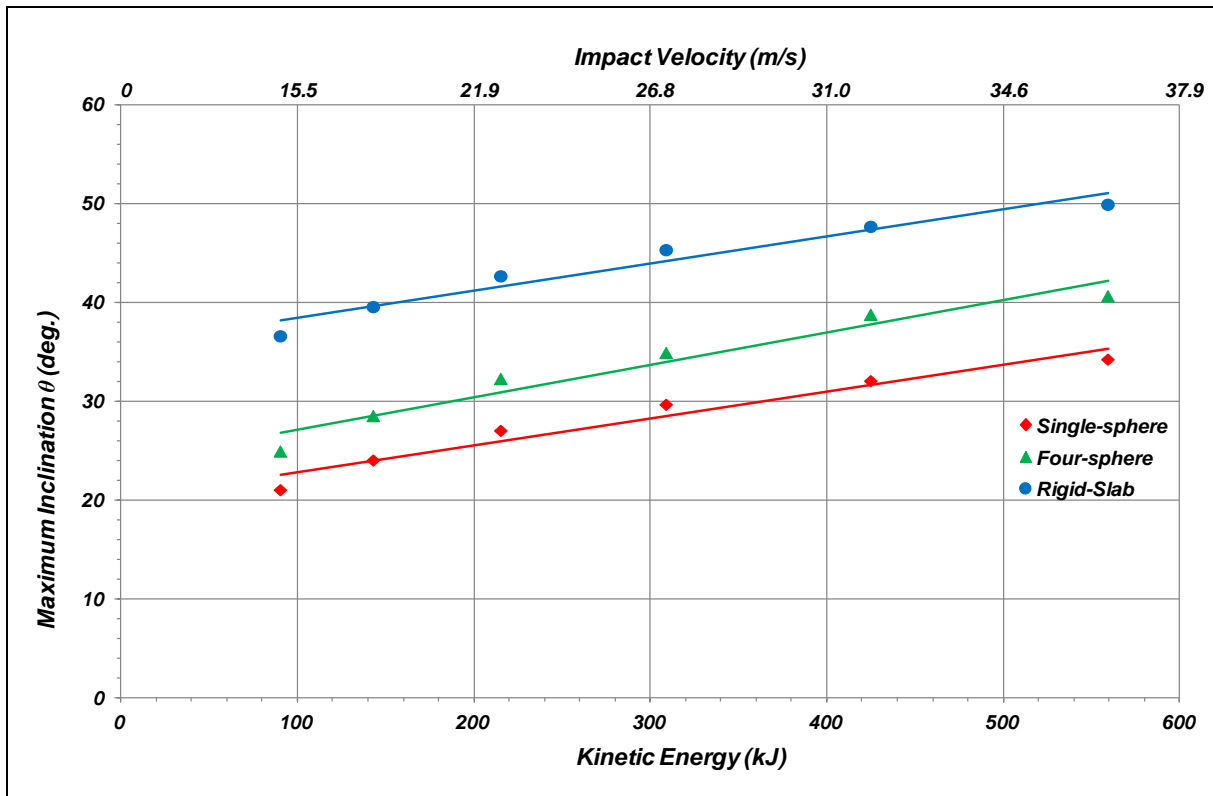
Figure 5.8   Maximum Inclination of Cables against Impact Velocity and Kinetic Energy

5.3   Barrier Deformation

According to the field observations of flexible debris-resisting barriers (Wendeler, 2013), landslide debris impact over a larger area of the barriers which result in less localised and small barrier deformations as compared with rockfall impact.   She opined that landslide debris impact could represent a less critical loading condition for barrier netting.

Figures 5.9 and 5.10 show the calculated maximum vertical deformation of the barriers and the maximum axial force of the ring net respectively in the LS-DYNA simulations.   The results echo the observations by Wendeler (2013).   Rigid-slab impacts produce a less critical barrier deformation and force in the ring net comparing with the impact of a single-sphere.
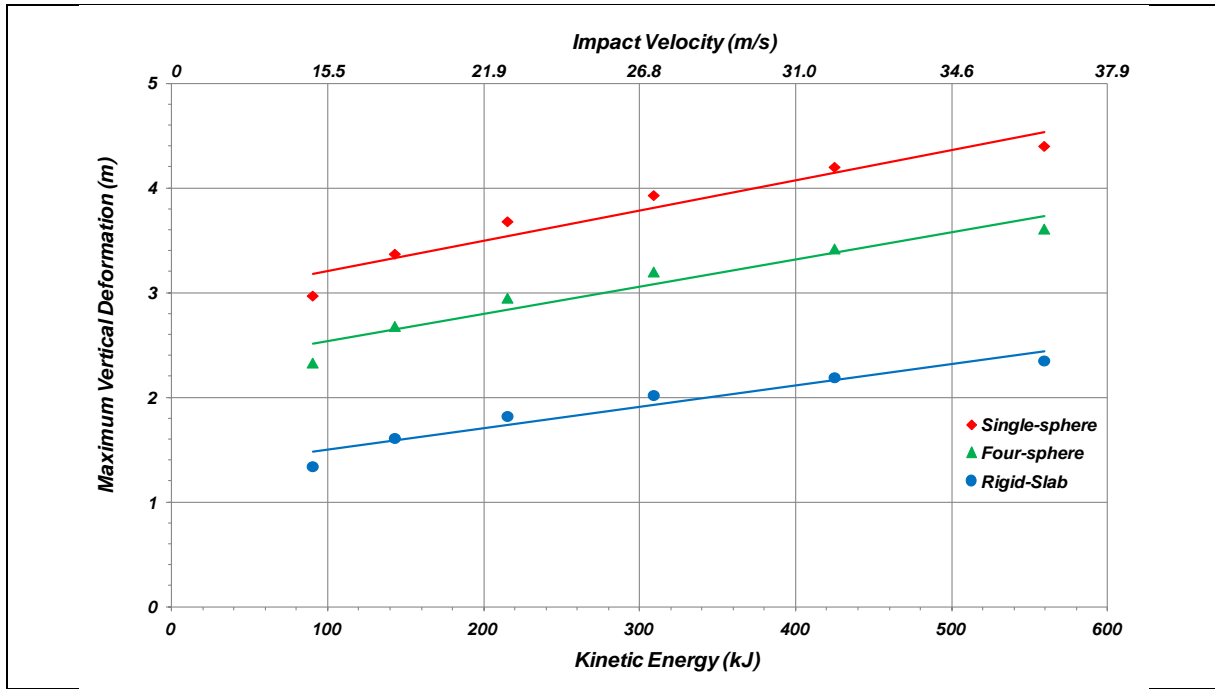
Figure 5.9   Maximum Vertical Deformations of Barriers
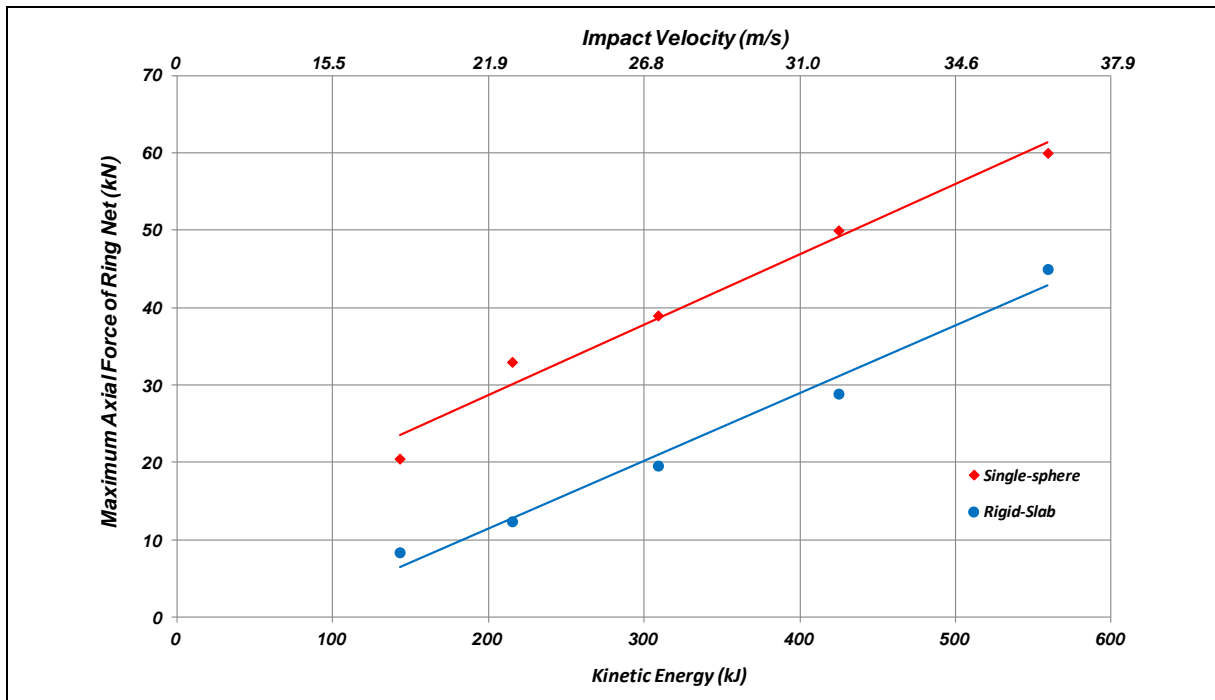
Figure 5.10   Maximum Axial Force in Ring Net

6   Numerical Study of Vertical Rockfall Barrier Subject to Punching and Areal Loads

6.1   General

The numerical studies presented in Section 5 pertain to a rockfall net laid horizontally.

In practice, flexible rockfall barrier systems are installed vertically or sub-vertically, and the steel posts are held in position by uphill and/or lateral cables.   Additional LS-DYNA simulations were thus undertaken to study the response of a vertical flexible rockfall barrier subject to punching and areal loads.

The LS-DYNA model set-up by Ng et al (2012) was adopted.   The model simulated the details of a 3,000 kJ proprietary flexible rockfall barrier system (Maccaferri, 2011).   In the model, the flexible barrier was 5 m high with five panels, 10 m wide each (Figure 6.1). Double cable ropes running along the top and bottom of the entire barrier respectively were anchored to the ground at both ends of the barrier.   The posts supporting the top cable rope and the net were held by tie-back retention cables.   The connection between the post and foundation was modelled as a pin joint.   Energy dissipating devices were installed along the cables.   Details of the numerical model can be found in Ng et al (2012).

Horizontal impact loads of a single-sphere weight and a rigid-slab weight were applied in the model analysis.   The size of the rigid slab was 7 m by 4 m.   The horizontal target impact kinetic energy was 3,000 kJ.   The weights of the single-sphere and rigid-slab were the same, viz. 4,400 kg.   The simulation schedule is presented in Table 6.1.

Figure 6.1   Flexible Rockfall Barrier System Subject to Impact of a Single-Sphere (Ng et al, 2012)

Table 6.1   Simulation Schedule for Study of Vertical Net

Simulation No.	Impact Weight	Dimension	Impact Velocity (m/s)	Kinetic Energy (kJ)
F1	Single-sphere	2.0 m dia.	37	3,000
F2	Rigid-slab	Each sphere: 1.0 m dia. Slab: 7 m by 4 m	37	3,000

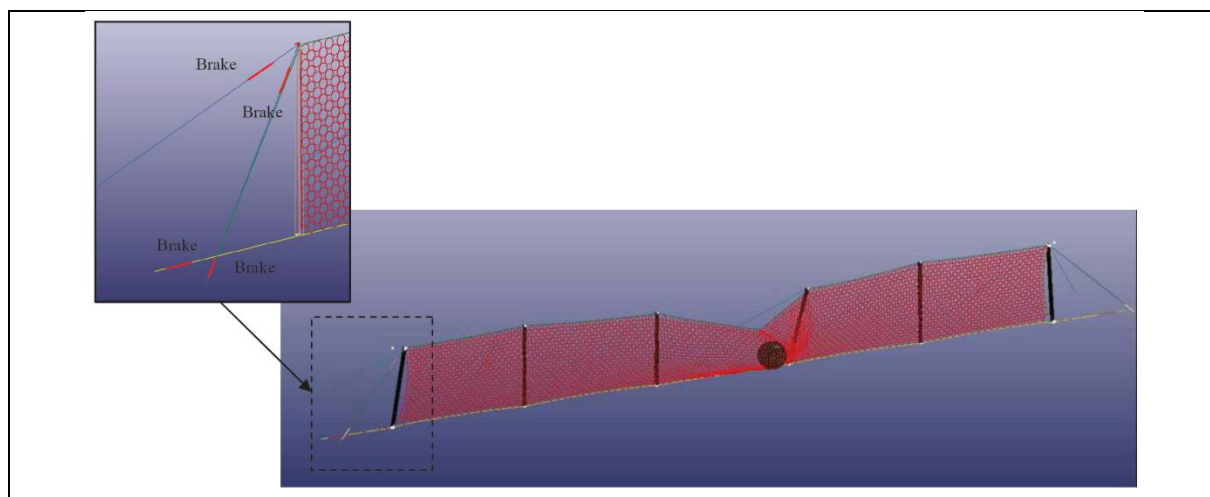## 6.2   Results of the Simulations

Figure 6.2 shows the graphical outputs of simulations for the single-sphere and rigid-slab weights, which depicts the deformed barrier from the instant when the impact weights touched the barrier until the maximum deformation was reached at about 0.4 to 0.45 seconds (see Figure 6.3).

The LS-DYNA simulations show that the rockfall barrier arrested the single-sphere and the rigid-slab.   The intermediate posts which were connected to the panel of netting of impact leaned forward.   Figure 6.3 shows the horizontal acceleration and displacement of the impact weights.   The time when the impact weights reached the barrier was taken as 0.0 second, and from that moment onward the impact weights experienced resistant forces from the barrier and started to decelerate.   The maximum decelerations of the rigid-slab and the single-sphere were 195 m/s^2 and 134 m/s^2 respectively.   Based on the Netwon's second law, it can be deduced that the rigid-slab experienced about 40% more resistance rendered by the barriers when compared with the single-sphere.   On the other hand, the single-sphere impact caused a larger net deformation.   The maximum horizontal displacements due to the single-sphere impact and the rigid-slab impact were 6.3 m and 5.1 m respectively.

Key results including cable forces and post reactions of the two simulations are summarised in Table 6.2.   Physical rockfall tests had been conducted for the proprietary rockfall barrier simulated in the LS-DYNA analysis in accordance with ETAG 27 requirements (Maccaferri, 2011).   Results of the physical test indicate that the maximum cable force induced by a 3,000 kJ rockfall impact was up to 293 kN and the maximum force in the uphill retention cable was 83 kN.   These are comparable with the results of the single-sphere simulation where the calculated maximum cable force and the calculated maximum uphill retention cable force were 225 kN and 60 kN respectively.   This demonstrates that the LS-DYNA model could replicate the response of the rockfall barrier satisfactorily.   The results of simulations could be further improved by adopting the exact barrier set-up, such as the orientation of the barrier posts, dimensions of panels and impact direction of single-sphere used the physical rockfall test.

The maximum forces developed in the cable ropes induced by the single-sphere and the rigid-slab impacts are comparable, since the cable force is dictated by the load-deformation characteristics of the brake elements.   The same is also observed for uphill retention cables (see Table 6.2).

The maximum post foundation shear force in the rigid-slab impact simulation was about 40% larger than that of the single-sphere impact.   This is consistent with the result presented in Section 5, i.e. as compared with single-sphere impact, rigid-slab impact could result in a more critical barrier foundation load in the direction of the impact.   The post foundation shear pertains to the horizontal component of the cable attached to the barrier post. It relates to the deflection angle of cables.   The larger the angle between the cable and the post, the greater is the post foundation shear (see Figures 6.4(a) and 6.4(b) and Table 6.2). Photography of the physical test of flexible debris-resisting barrier is also included in Figure 6.4(c) for qualitative comparison purposes.   On the other hand, the rigid-slab impact could result in a smaller vertical reaction (i.e. bearing pressure) on the post foundation.   If shallow foundation is used to support the barrier post, the rigid-slab impact could give rise to a larger sliding force compared with the single-sphere impact.

Single-sphere	Rigid-slab
t = 0 sec.	t = 0 sec.
t = 0.2 sec.	t = 0.2 sec.
6.3 m t = 0.4 sec.	5.1 m t = 0.4 sec.
t = 0.6 sec.	t = 0.6 sec.
t = 0.8 sec.	t = 0.8 sec.
t = 1.0 sec.	t = 1.0 sec.
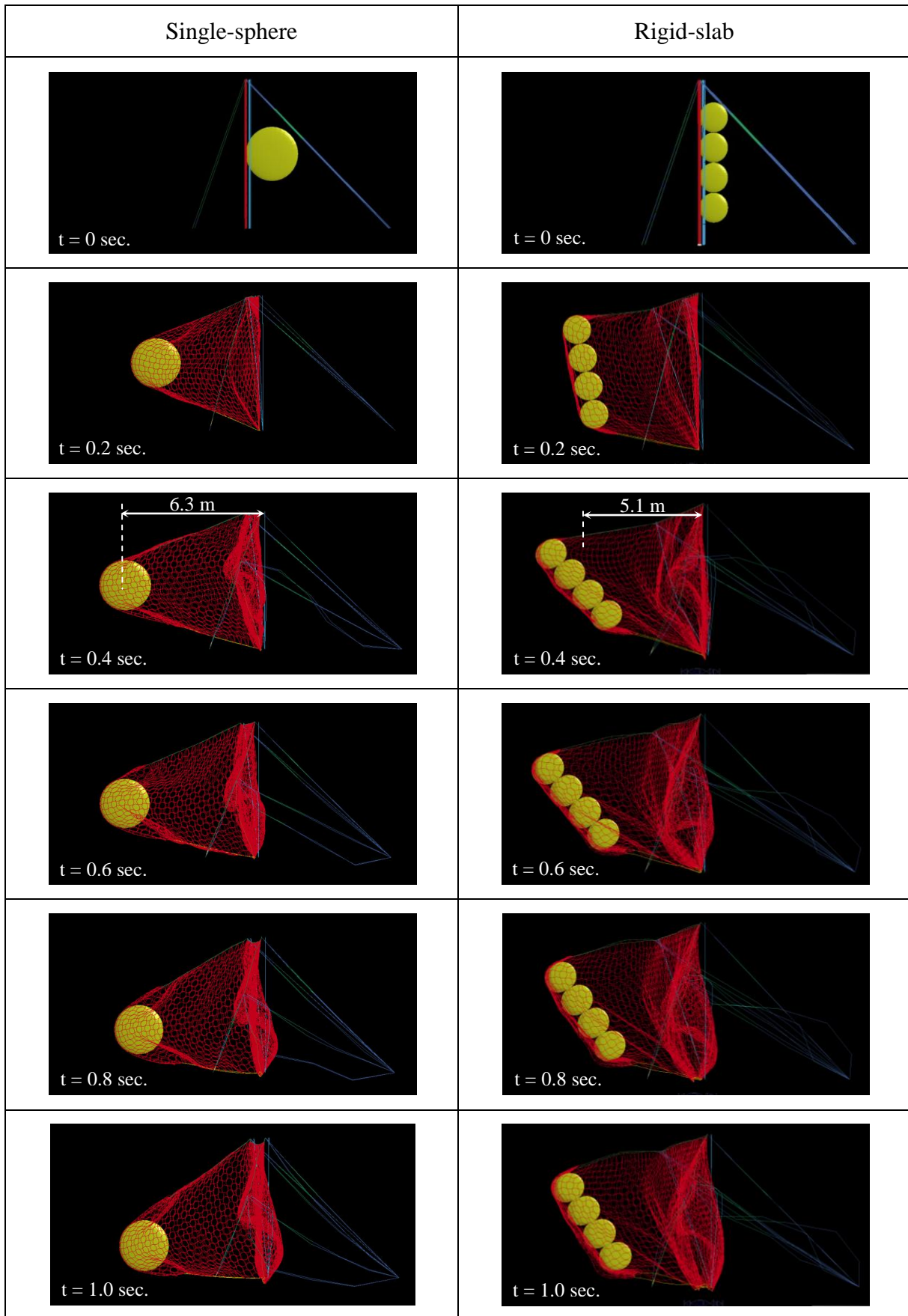
Figure 6.2   Graphical Outputs of the Numerical Simulations
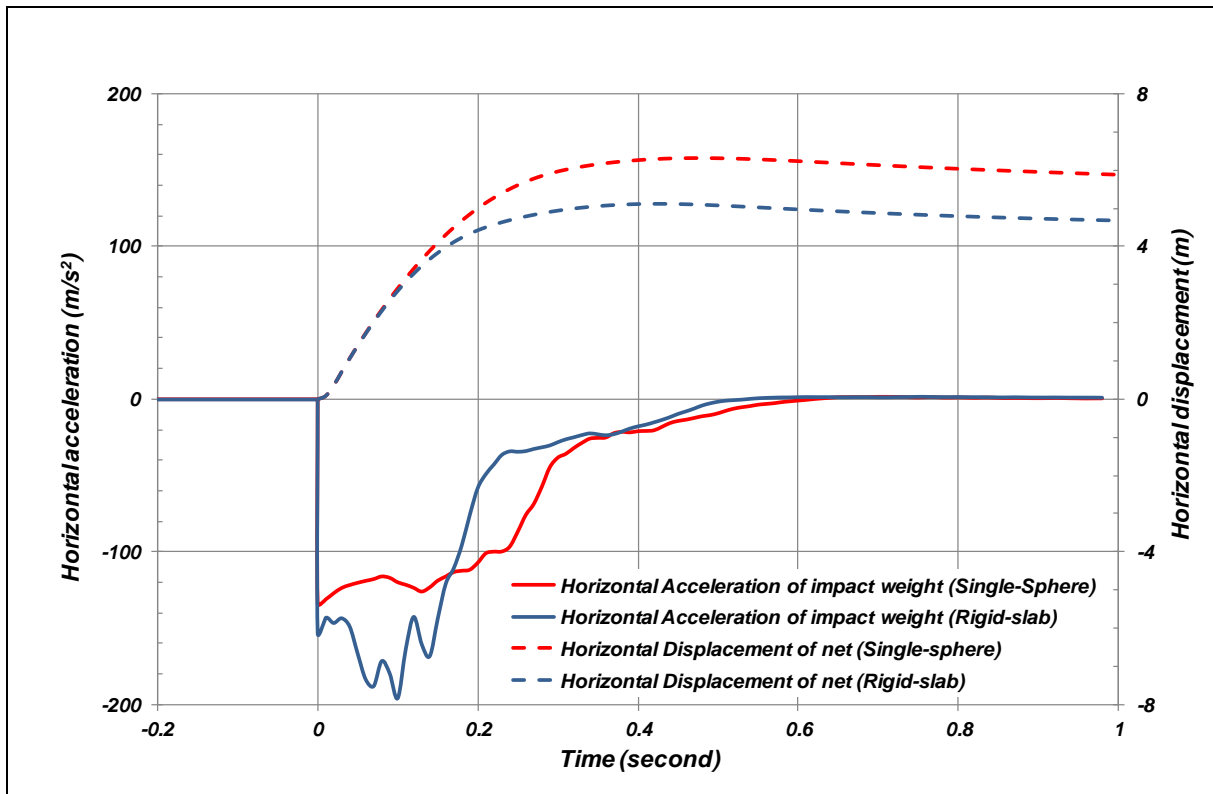
Figure 6.3 **Horizontal Acceleration and Horizontal Displacement of the Impact Weights**

Table 6.2 **Key Results - Maximum Forces, Cable Inclination and Barrier Deformation**

	Single-sphere	Rigid-slab	Difference
Top cable force	225 kN (per cable rope)	242 kN (per cable rope)	+8%
Bottom cable force	117 kN (per cable rope)	152 kN (per cable rope)	+30%
Uphill retention cable force	60 kN (per cable rope)	65 kN (per cable rope)	+8%
Shear at post foundation	190 kN	259 kN	+36%
Vertical reaction at post foundation	181 kN	150 kN	-21%
Deflection angle of cable (θ) (see Figure 6.4)	30°	50°	+67%

(a) Deflection angle of cable (Single-sphere)   (b) Deflection angle of cable (Rigid-slab)

(c) Physical test of landslide-debris barrier (Geobrugg, 2010)
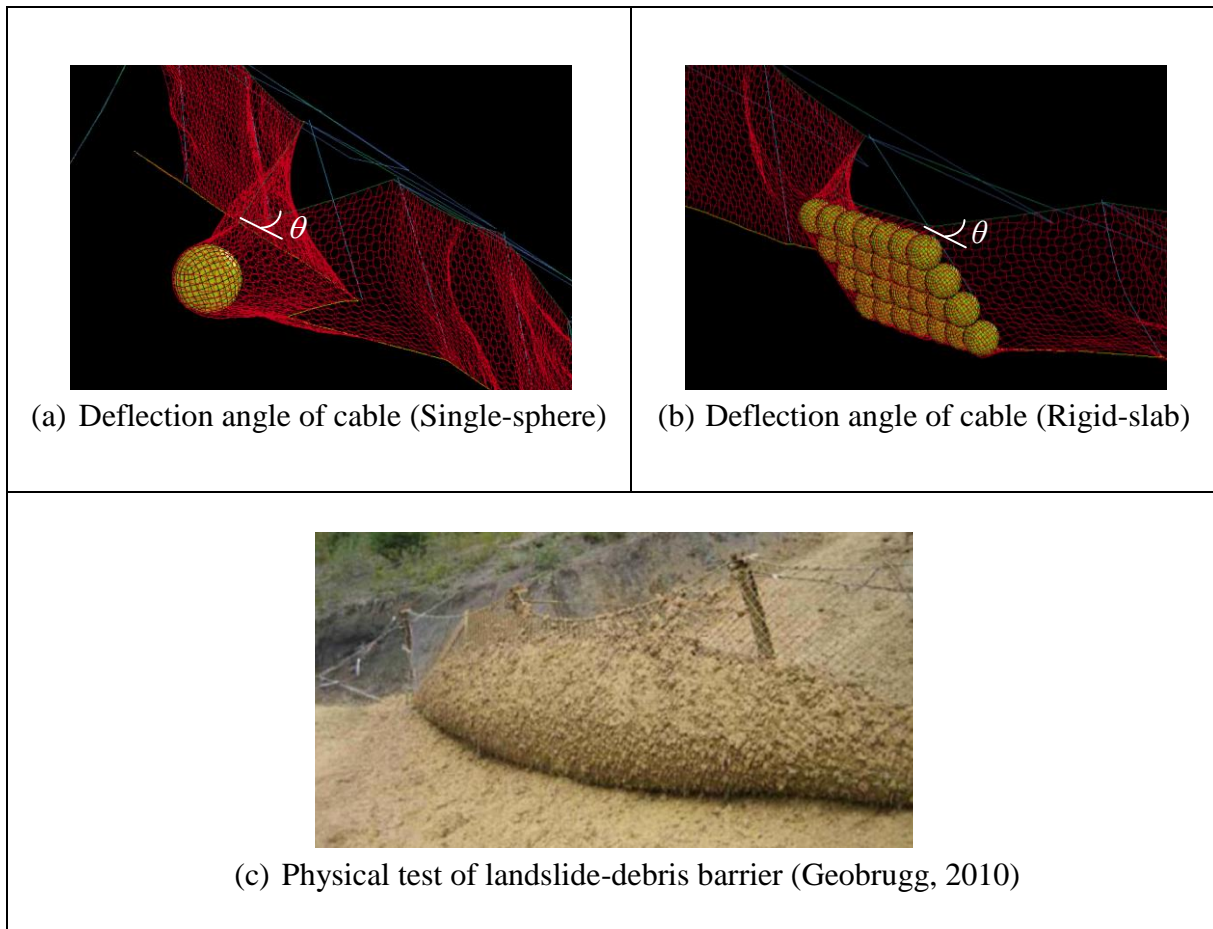
Figure 6.4   Deflection Angle of Cables

Forces and bending moments developed in the barrier post are presented in Table 6.3. LS-DYNA simulations reveal that the post bending moment induced by the areal impact load and the punching impact load may be comparable in order, while the areal impact load could result in a smaller post axial load.

Table 6.3   Maximum Bending Moments and Axial Forces in Barrier Posts

	Single-sphere	Rigid-slab	Difference
Maximum bending moment in posts	36 kNm	40 kNm	+11%
Maximum axial compressive load in posts	285 kN	229 kN	-24%

7 Discussion

Numerical studies of the responses of two flexible rockfall structures with details reported by Volkwein (2004) and Maccaferri (2011) respectively had been conducted. The results show that the two rockfall structures could withstand the impact of the rigid-slab, which simulated landslide debris impact, with the kinetic energy same as their energy capacity. This seems to provide additional support for the use of flexible rockfall barrier to resist landslide debris.

The present study shows that movement of netting along the cables to which it attaches could play an important role in the internal load transfer mechanism of the barrier structure. The netting movement could control the angle between the cable and barrier posts, and hence the magnitude of load transferred to the post foundation. The results of the LS-DYNA analyses indicate that the foundation load in the impact direction induced by an areal impact load could be about 40% higher than that of a punching impact load. However, it must be emphasised that the areal load created by the rigid-slab may not accurately simulate the impact of landslide debris for the following reasons:

(a) The rigid-slab is taken to be infinitely rigid in the LS-DYNA analysis whereas landslide debris actually deforms during impact, and the deformation would lead to energy dissipation and a different configuration of movement of the netting.

(b) Landside debris normally hits barriers in surges over a certain duration, however, the rigid-slab adopted in the numerical simulations produces only a single impact with loaded area covering about 70% of the a barrier panel.

(c) The sequential deposition mechanism of landslide debris behind the barrier, which may help resisting debris impact from behind, is not simulated.

All in all, the rigid-slab impact would create a loading condition more critical than the impact of landslide debris which is deformable. The bulging at the upper part of the ring net caused by the rigid-slab impact as observed in the numerical analysis of the vertical barrier results in a larger elongation of top cable comparing with field situations. On the other hand, the effects of small particles and water passing through the mesh (see Figure 6.4(c)) are not considered in the present numerical study.

In current practice, design foundation load of rockfall barriers is established based on the peak cable force measured in full-scale physical tests. Recent study by Knonau (2011) recommended that a load factor of at least 1.5 should be allowed for. This load factor could provide a safety margin to cater for the uncertainty of impacting angle and dimensions of rock.

Despite the above, it should be cautioned that the performance of the rockfall barrier simulated by the numerical analysis was idealized in the simulation. Possible malfunctioning of some barrier components due to external factors (e.g. burying of cables

and/or energy dissipating devices by landslide debris) have not been considered in the numerical analysis.   If any cables/energy dissipating devices are buried by landslide debris, their movements could be restrained and this could adversely affect the barriers' overall performance.   These scenarios can have significant implications to the robustness of flexible barriers.   Yet they cannot be easily simulated numerically.

The load transfer mechanism between different components of the flexible barrier structure can dictate the performance of the barrier.   Therefore, observations made by this study may not be relevant to other rockfall barriers with structural design different from the two barriers assessed in this study.   In addition, the scenario of landslide debris impacting directly on barrier post has not been studied.

8   Further Work

Numerical analyses conducted in this study consider impact of discrete objects on rockfall barriers.   The impact of deformable landslide debris in form of surges cannot be simulated using this approach.   In addition, the mass of the drop weights is less than that considered in designs.   Possible further work may include modelling of landslide debris as a continuum material, and the volume of the landslide event should be comparable with designs in practice.   Modelling of other common types of flexible barriers in Hong Kong with different structural setting in future study would be worthwhile.

9   Conclusions

Performance of two flexible rockfall barriers in resisting punching and areal loads has been investigated using a non-linear finite element program LS-DYNA.   Structural details of the two flexible rockfall barriers were presented by Volkwein (2004) and Maccaferri (2011).   The numerical analyses show that the two rockfall barrier structures could withstand the impact of a rigid-slab with the kinetic energy same as their energy capacity.

However, the results of the LS-DYNA analyses indicate that the barrier foundation load in the direction of impact induced by areal load could be about 40% higher than that of punching impact load of single sphere impact.   This value is considered to be on the high side, as the rigid-slab is non-deformable.

10   References

Arup (2013).   *Pilot Numerical Investigation of the Interactions between Landslide Debris and Flexible Debris-Resisting Barriers, Interim Report No. 1*.   Report prepared for Geotechnical Engineering Office, Hong Kong, 70 p.

Chan, S.L., Zhou, Z.H. & Liu, Y.P. (2012).   Numerical analysis and design of flexible barriers allowing for sliding nodes and large deflection effects.   *Proceedings of the One Day Seminar on Natural Terrain Hazards Mitigation Measures*, 16 October 2012, Hong Kong, pp 29-43.

Duffy, J.D. (1998). Case studies on debris and mudslide barriers systems in California. *Proceedings of the One Day Seminar on Planning, Design and Implementation of Debris Flow and Rockfall Hazards Mitigation Measures*, 27 October 1998, Hong Kong, pp 77-90.

EOTA (2008). *Guideline For European Technical Approval of Falling Rock Protection Kits*. European Organisation for Technical Approvals (EOTA), 53 p.

Geobrugg (2007). *Debris Flow Barriers: Debris Flow Test Site Illgraben*, VS/Switzerland. Technical Documentation, September 2007, Geobrugg, 12 p.

Geobrugg (2009). *Falling Rock Protection Kit for Use in Civil Engineering Works to Stop Moving Rock Blocks with Maximum Energy Level of 3,000 kJ, ETA – 10/0084*, European Technical Approval, 30 p.

Geobrugg (2010). *Debris Flow Protection in Areas of the Pyrenees: Behaviour of VX Barriers and Initial Results from the Pioneer Monitoring Station in Erill and Portainè*, Spain. Technical Documentation, October 2010, Geobrugg, 16 p.

Grassl, H.G. (2002). *Experimentelle und numerische Modellierung des dynamischen Frag- und Vergormungsverhaltens von hochflexiblen Schutzsystemen gegen Steinschlag*. PhD Thesis, Technical Sciences of the Swiss Federal Institute of Technology Zurich, 156 p. (in German)

Knonau, M. (2011). *Anchorings and Foundations of Rockfall Safety Nets*. Report No. 11-05, Swiss Federal Research Institute, 32 p.

Kwan, J.S.H. & Koo, R.C.H. (2013). *Preliminary Back Analysis of Open Hillside Landslide Impacting on a Flexible Rockfall Barrier at Jordan Valley (SPR 1/2013)*. Geotechnical Engineering Office, Hong Kong, 56 p.

Maccaferri (2011). *ETA Rockfall Testing Report for Maccaferri Flexible Barrier RMC300A,* Maccaferri, 55 p.

Margreth, S. & Roth, A. (2008). Interaction of flexible rockfall barriers with avalanches and snow pressure. *Cold Regions Science and Technology*, vol. 51, pp 168-177.

Ng, A.K.L., Williamson, S.J. & Chong, A.K.T. (2012). Developments in design considerations and use of flexible barriers as mitigation measures for channelised debris flow and open hillslope failures - a case study. *Proceedings of the One Day Seminar on Natural Terrain Hazard Mitigation Measures*. AGS, Hong Kong, pp 61-66.

Nicot, F., Cambou, B., Mazzoleni, G. (2001). From a constitutive modeling of metallic rings to the design of rockfall resisting nets. *International Journal of Numerical Analysis Methods of Geomechanics,* vol. 25, pp 49-70.

Roth, A., Kästli, A. & Frenez, Th. (2004). Debris flow mitigation by means of flexible barriers. *Proceedings of the International Symposium Interpraevent 2004*, Trento, Italy, 12 p.

Tang, D., Berger, G., Toniolo, M., Shen, J.M. & Kung, D. (2009).   A new flexible barrier system for Hong Kong.   *Proceedings of the Twenty-ninth Annual Seminar - Natural Hillsides: Study and Risk Mitigation Measures*, Geotechnical Division, The Hong Kong Institution of Engineers, pp 55-60.

Volkwein, A. (2004).   *Numerical Simulation of Flexible Rockfall Protection Systems*.   PhD Thesis, Swiss Federal Institute of Technology Zürich, Switzerland, 134 p. (in German)

Wendeler, C. (2013).   Personal communications.

Wendeler, C., McArdell, B.W., Rickenmann, D., Volkwein, A., Roth, A. & Denk, M. (2006).   Field testing and numerical modelling of flexible debris flow barriers.   *Proceedings of the Sixth International Conference of Physical Modelling in Geotechnics*, 4-6 August 2006, Hong Kong, pp 1573-1604.

WSL (2009).   *Full-Scale Testing and Dimensioning of Flexible Debris Flow Barriers*.   Swiss Federal Institute for Forest, Snow and Landscape Research (WSL), 22 p.

WSL (2010).   *Report on Testing SL-100 a Protection System against Shallow landslides, Test Report No. 10-15*.   Swiss Federal Institute for Forest, Snow and Landscape Research (WSL), 13 p.

Zhou, Z.H., Liu, Y.P. & Chan, S.L. (2011).   *Nonlinear Finite Element Analysis and Design of Flexible Barrier (Project Report)*.   The Hong Kong Polytechnic University, 26 p.

Appendix A

Numerical Model Developed by Arup (2013)

Contents

List of Tables

List of Figures

A.1 Set-up of the Physical Field Test Model

Arup (2013) carried out LS-DYNA analysis to repeat numerically the rockfall tests reported by Grassl (2002) and Volkwein (2004).   Detailed set-up of the rockfall tests is presented in Figure A1.   The test rig consisted of a steel frame structure 4.69 m high as measured from the top of the concrete block footing.   The plan dimensions of the test rig were approximately 5 m long by 5 m wide.   There were 4 nos. of 22 mm diameter steel cables running along each side of the test rig which draped the flexible ring net in place. These cables were supported on the steel frame of the test rig through a smooth pulley system and each of the cables was pre-stressed to a tension of 10 kN.   Figure A2 shows the pulley system.   Towards each end of the anchorage block, a single brake ring as energy dissipating devices was connected to each cable.   Sensors were also installed on the cables near the anchor blocks to measure the tension load developed in the cables during the tests.

The flexible ring net was made of Rocco 07/3/300 rings.   The 300 mm diameter rings were formed by 7 nos. winding of 3mm diameter steel wire of ultimate tensile stress of 1,770 MPa.   These rings were able to slide freely against each other.   The flexible ring net was connected to the steel cables via ¾ " (~19 mm) shackles.   These shackles allow the edge rings to move along the cable direction.   Figures A3 to A5 show samples of various structural components of the system including the brake rings (originally extracted from Volkwein, 2004).

In the Volkwein field testing, an 820 mm diameter ball made of high performance concrete with steel fibre was dropped from 16 m and 32 m to simulate the rockfall scenarios. The total mass of the weight was 825 kg.   Acceleration measurement devices were installed in the concrete ball.   High speed video cameras were used to capture the motion of the concrete ball and the deformation of the net.   Various tension and pressure sensors were installed to measure the forces and pressure developed in different structural components of the test rig.

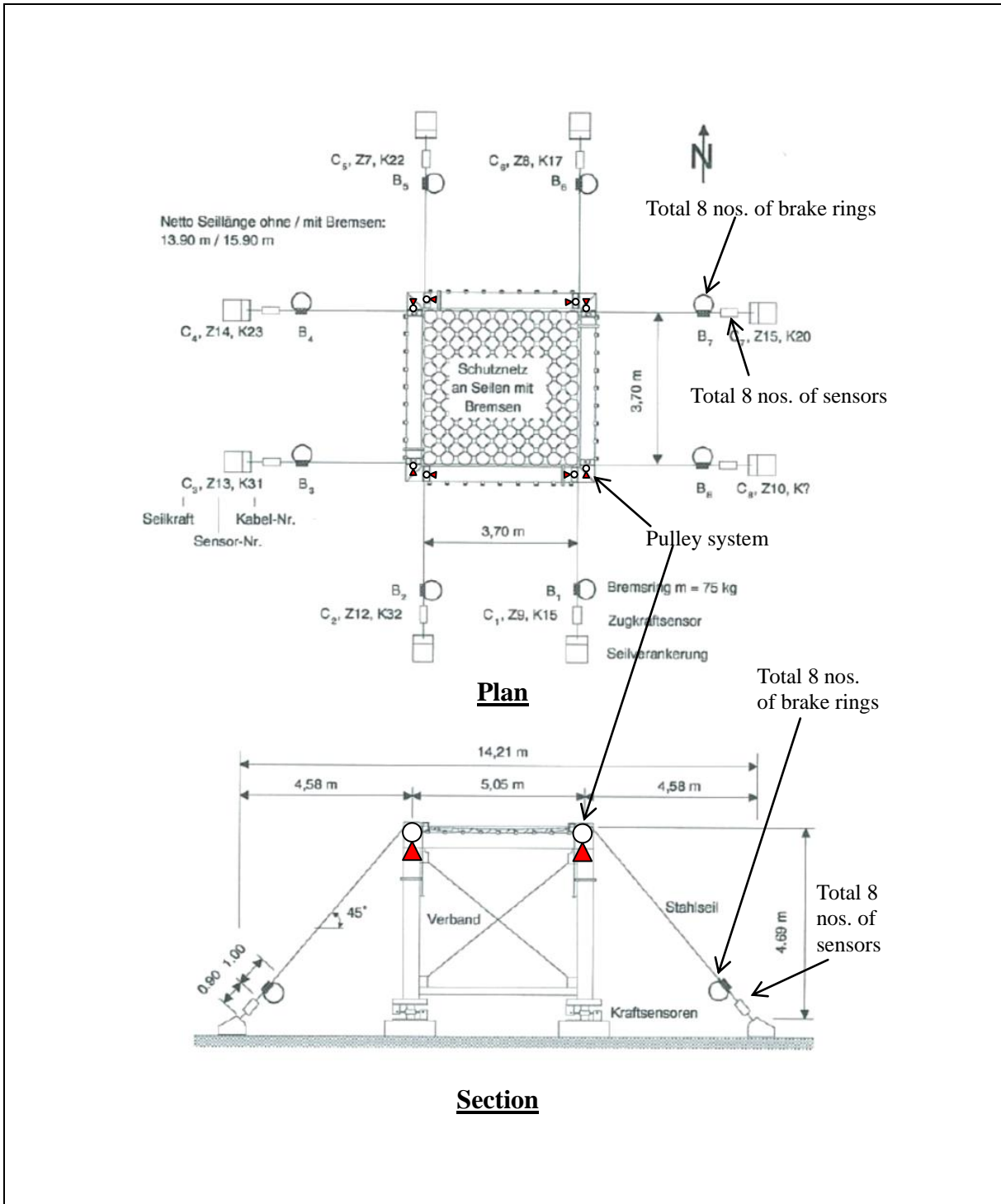**Figure A1   Test Set-up of the Flexible Rockfall Barrier System (Volkwein, 2004)**
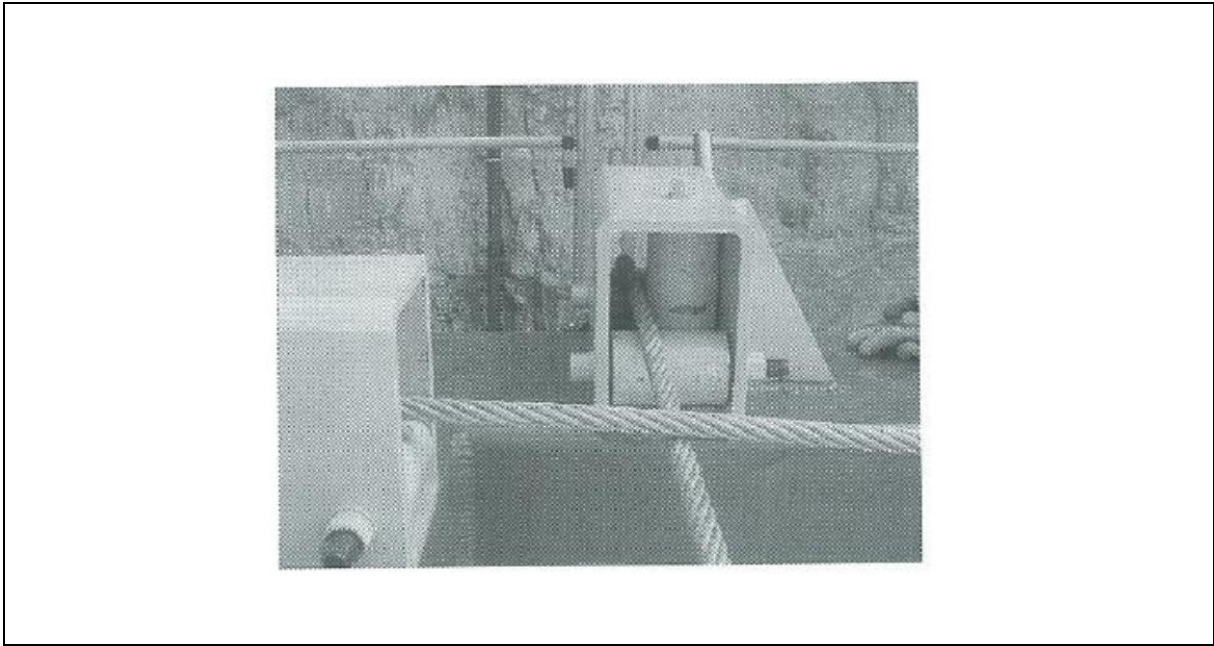
Figure A2   Smooth Pulley Systems that Supported the Steel Cable on the Test Rig (Volkwein, 2004)
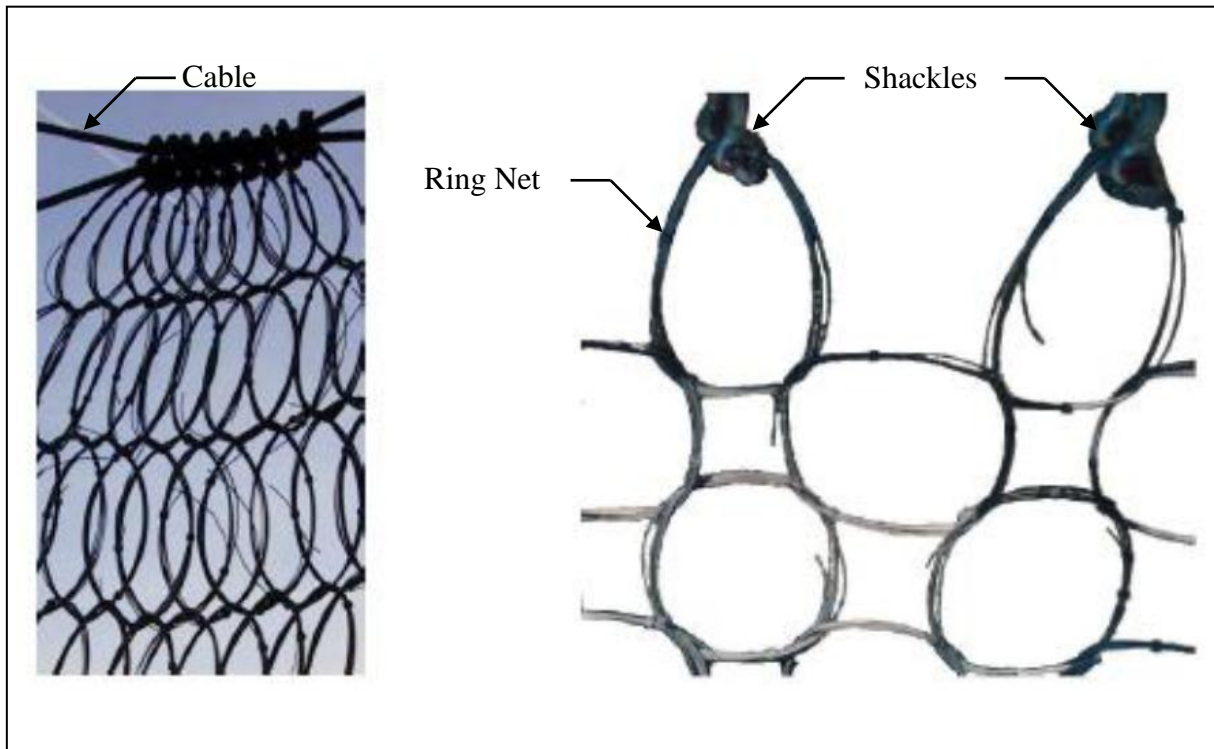

Figure A3   Net Rings, Steel Cable and Shackles (Volkwein, 2004)

Figure A4   Windings of Steel Wires Forming Rings

Figure A5   (Top) Brake Ring in its Original Shape; and (Bottom) Deformed Brake Ring Subject to Tension Load

A.2 Numerical Model Set-up

The steel frame of the test rig in the LS-DYNA simulation (Arup, 2013) is supported by pin joints (see red triangles shown in Figure A1).   The pulley system above the pin joint is simulated using LS-DYNA "seat-belt" element as shown in Figures A1 and A2 which allows smooth sliding of the steel cables on the steel frame structure.

Figure A6 shows the LS-DYNA model for the set-up of ring nets.   All other structural components including the cable, shackles, brake rings and ring net are explicitly modelled using beam elements.   Figures A7 and A8 provide graphical illustrations of the beam elements representing the net rings and shackles, which can slide/move relative to each others. No movement is allowed at the end of each steel cable where the cable was connected to the concrete anchor block in the rockfall test.

The concrete drop ball is modelled as a rigid sphere in the LS-DYNA model.   The weight of the drop ball is the same as that reported by Volkwein (2004).   The concrete ball is assigned to stay at the appropriate height above the test rig as per the actual test configuration.
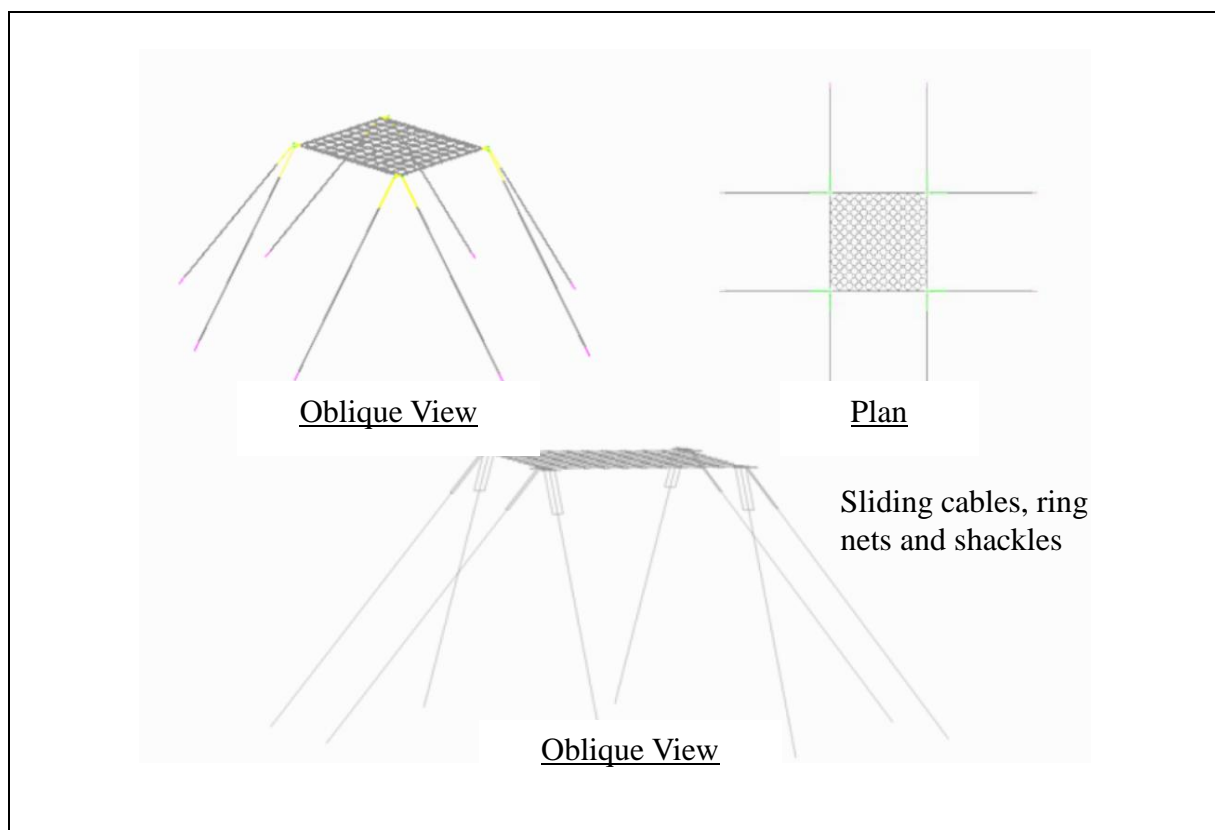

Oblique View

Plan

Sliding cables, ring nets and shackles

Oblique View

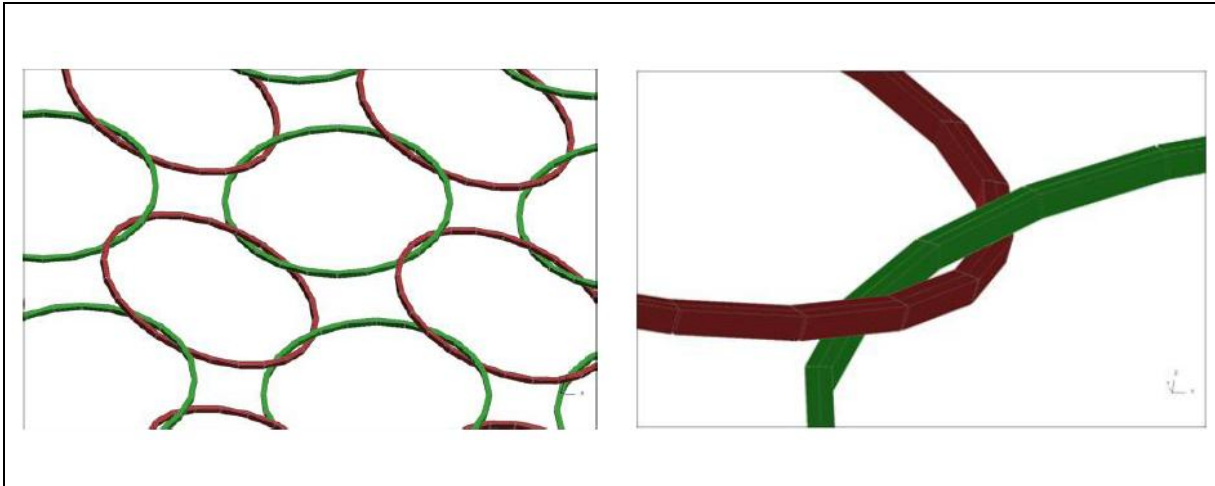**Figure A6   Ring Net Set-up to the Field Test Model of Volkwein (2004)**

Figure A7   Explicit Modeling of Net Rings in LS-DYNA (Arup, 2013)
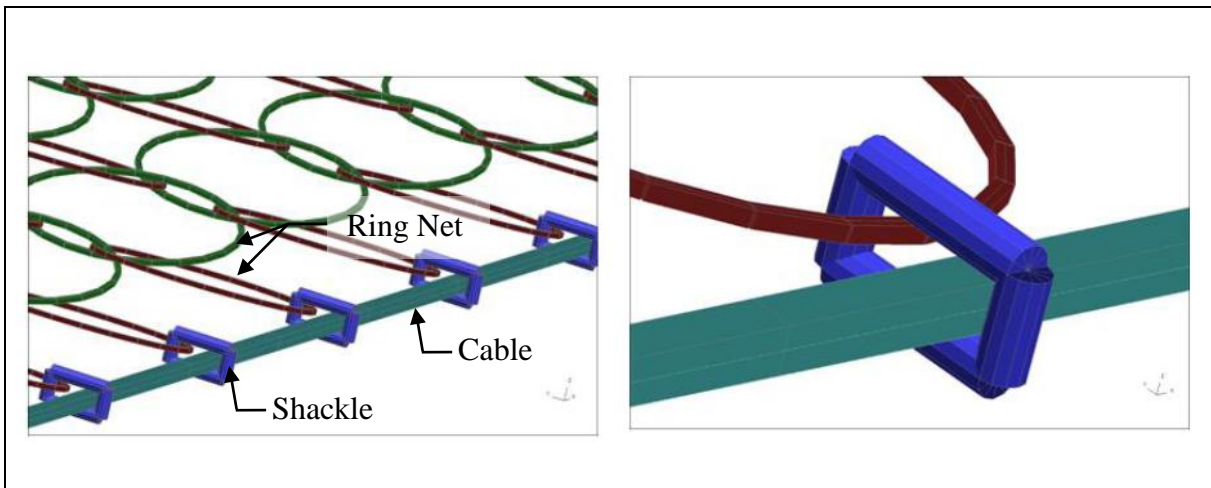
Figure A8   Connections among Net Rings, Shackles and Cables (Arup, 2013)

A.3   Materials and Parameters Used

A number of the structural components of the test rig exhibit highly non-linear behavior, such as net rings and brake rings.   The appropriateness of the ring parameters derivation is confirmed by carrying out a validation run that simulated the four-point pulling test (Test R3) on a single Rocco ring 12/3/300 as shown in Figure A9 by Volkwein (2004). Figure A9 shows the comparison of the LS-DYNA model results with the test data reported by Volkwein (2004).   It can be seen that when the ring is stretched, it will deform in bending mode and then followed by tension mode.   The LS-DYNA simulates the ring and the load-deformation characteristic of the ring explicitly.   Table A1 summarises the structural properties adopted in modelling the Rocco ring.
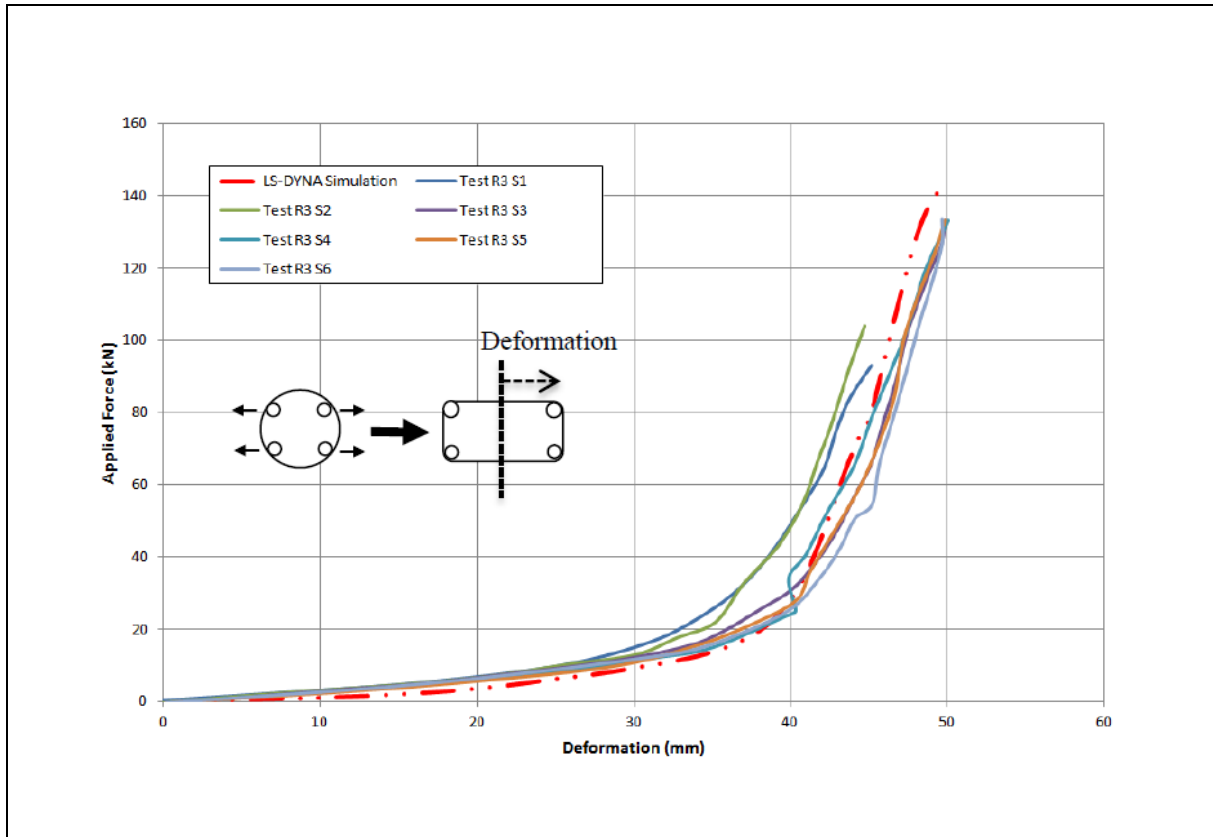
Figure A9   Four-point Pulling Test of Single Rocco Ring 12/3/300; Comparison between LS-DYNA Simulation Results and Test Data Reported by Volkwein (2004)

Table A1   Input Parameters for Rocco 7/3/300 Net Rings in LS-DYNA (Arup, 2013)

Material Property	Adopted Input Parameters
Material density, R_0	7800 kg/m^3
Elastic modulus, E	200 GPa
Poisson's ratio, PR	0.3
Cross-sectional area, A	4.95 x 10^{-5} m^2
Second moment of area, I	2.78 x 10^{-11} m^4

The load-deformation curve for the brake ring element is determined based on information given in Volkwein (2004) (see Figure A10).   The brake ring type GS8002, which shows a stiffer response than type GS8001 is used for the 32 m drop test.   The type GS8001 brake ring has been adopted in this numerical study.   Structural properties of brake rings and cables are summarised in Table A2.

Figure A10   Load-Deformation Relationship Curve of Brake Ring (Arup, 2013)

Table A2   Input Parameters for Steel Cables and Brake Rings in LS-DYNA (Arup, 2013)
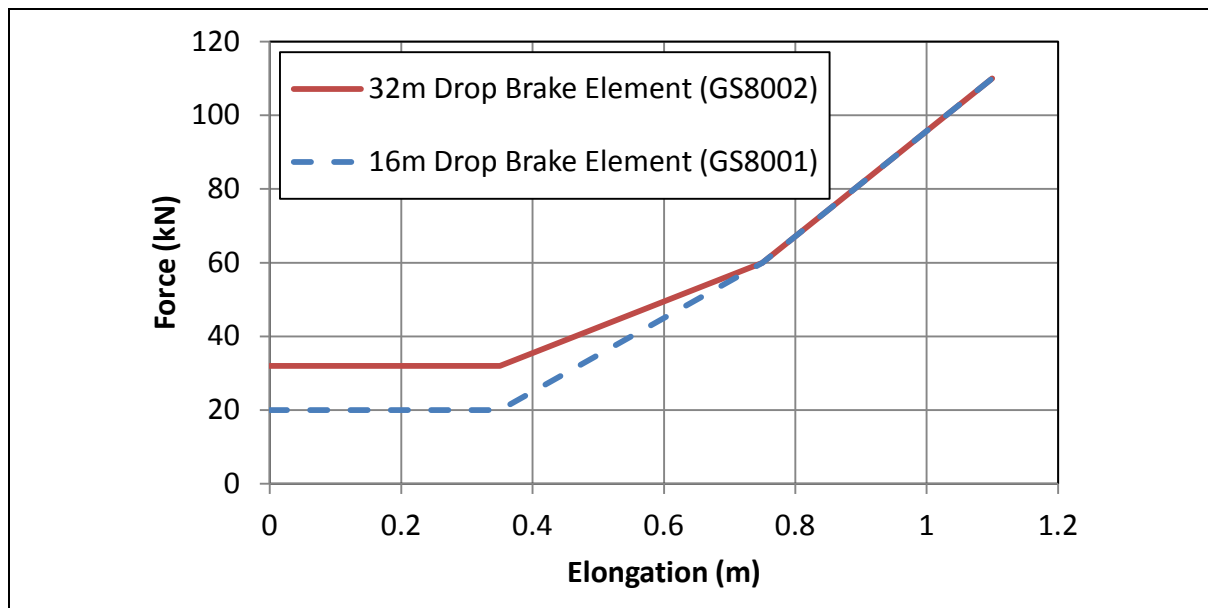
Material Property	Adopted Input Parameters	Remarks
Material density, R_0	7800 kg/m^3	-
Elastic modulus, E	100 GPa	-
Poisson's ratio, PR	0.3	-
Cross-sectional area, A	3.8 x 10^{-4} m^2	-
Second moment of area, I	7.0 x 10^{-10} m^4	Adjusted for the difference in metallic cross sectional area and full cross sectional area

The steel cables are modelled as linearly elastic material in the LS-DYNA simulation. Since the cables are made of multiple number of steel wires stranded together, its metallic cross sectional area would be smaller than the full cross sectional area.   The elastic modulus therefore is adjusted to reflect such a difference.   Volkwein (2004) suggested the range of elastic modulus was 70 GPa to 170 GPa.   An elastic modulus of 100 GPa has been adopted in the LS-DYNA simulation.   Table A2 summarises the material parameters adopted for steel cables.   No test data on the contact friction between different components of the test rigs are available.   Volkwein (2004) suggested a friction coefficient of μ = 0.1 for cable friction from the observed results of the low energy physical tests.   Grassl (2002) recommended that the reasonable range of friction coefficient between structural components would be 0 to 0.15. A friction coefficient of μ = 0.1 has been adopted for all material contacts by Arup (2013).

A.4 Numerical Modelling Procedures

The LS-DYNA model is initialised by applying gravity to all structural elements in the computation domain including the test rigs and the concrete ball. The concrete ball is initially held at a fixed position of 16 m or 32 m above the test rig and refrained from dropping downwards. As gravitational force was applied to the test rig, the ring net would sag naturally as it would be in reality. Damping is then applied for 2 seconds to enable the ring net to settle down to avoid any excessive vibration. Afterwards, the concrete ball was allowed to fall freely and impact on the flexible barrier. The position, velocity and potential energy of the concrete ball were tracked and recorded. The deformation of the ring net and the movement of the steel cables are calculated. In addition, the tension force developed within the steel cables is recorded.

A.5 Verification against Physical Test Results

The following results have been compared with the physical rockfall test data reported by Volkwein (2004):

> (a) The position of the ball with respect to time.
>
> (b) The total energy of the ball with respect to time.
>
> (c) The cable force with respect to time.

The results for the cases of 16 m and 32 m drops for flexible barriers with brake rings are shown in Figure A11. The instant when the ball reached the elevation of the test rig ring net is denoted by $t = 0$ second. Figure A11(a) demonstrates that the LS-DYNA analysis is able to simulate the ball displacement measured in the physical test by Volkwein (2004). The estimated energy dissipation of the drop ball and tensile forces developed in the cables by LS-DYNA also agree well with those measured in the physical tests (see Figures A11(b) and A11(c)). It is demonstrated that the LS-DYNA structural modelling of the flexible barrier is able to replicate the nonlinear behaviour of the flexible barrier subject to impacts.

Also, as demonstrated in Figure A12, the explicit modelling of the structural components in LS-DYNA, for example, free sliding of net rings and shackles, enables accurate predictions of the movements of the ring net and the plastic deformation of rings. The extension and sideways movement of the steel cables have also been simulated accurately and they are in good agreement with the physical test results and the overall deformation of the barrier.
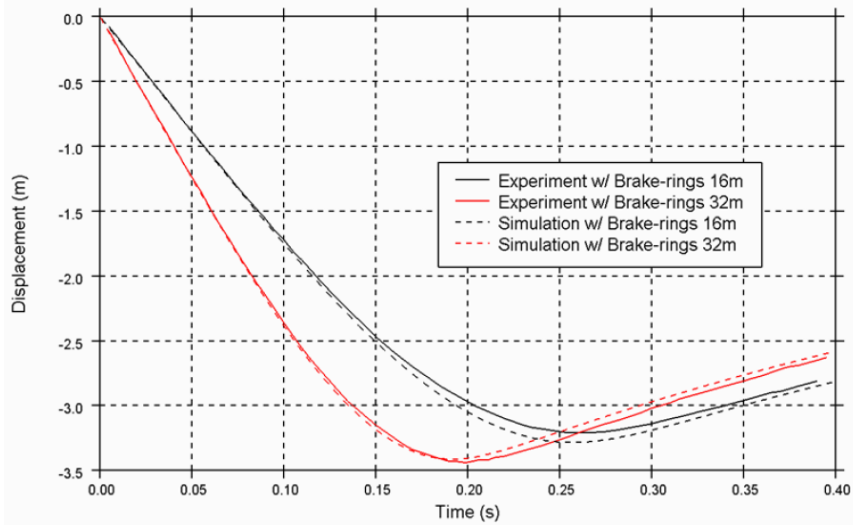
(a) Displacement-time curves of vertical position of the concrete ball
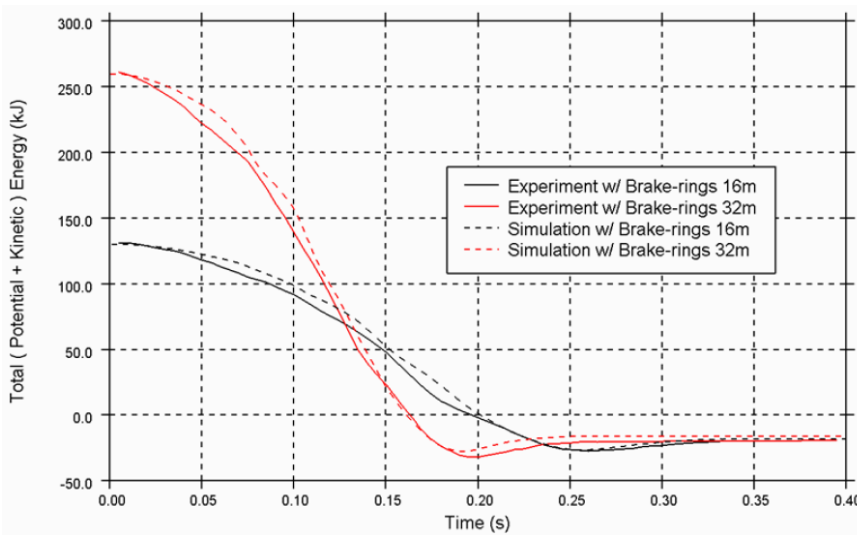
(b) Total energy-time curves of vertical position of the concrete ball
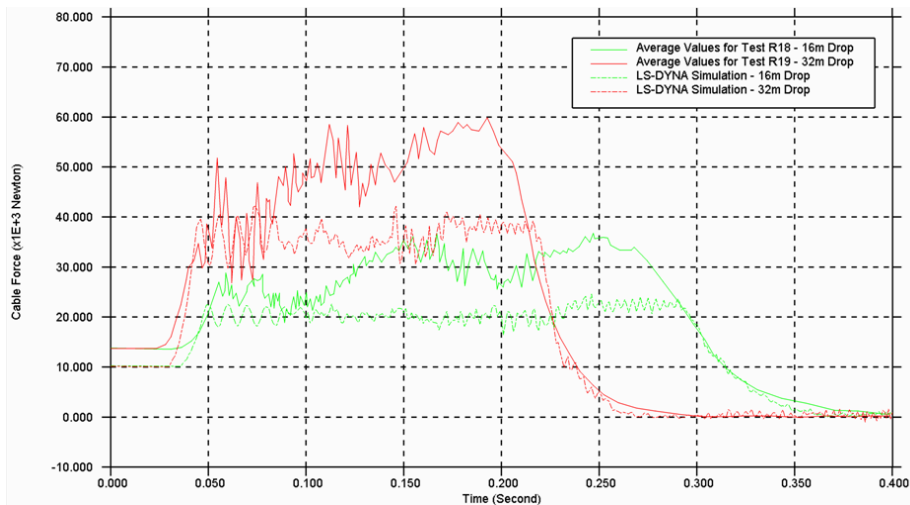
(c) Cable force-time curves of vertical position of the concrete ball

Figure A11   Comparison between Results of LS-DYNA Simulations and Physical Rockfall Tests

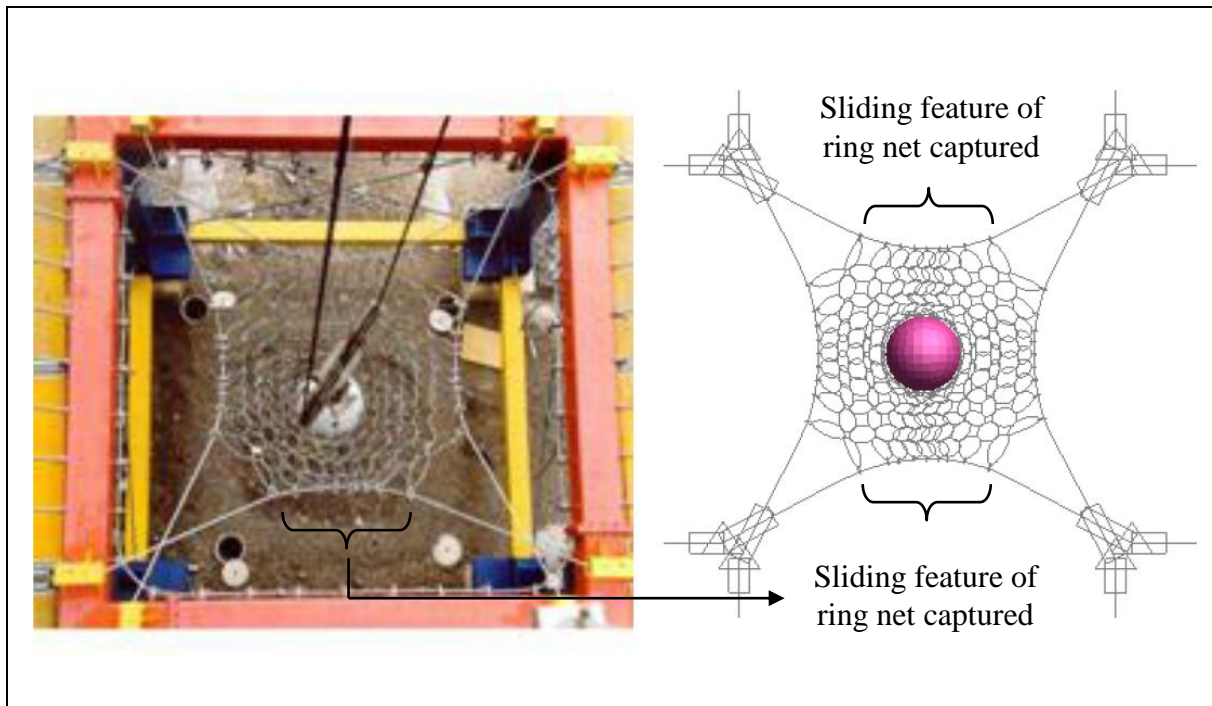**Figure A12   (Right) Plan View on the Final Position of the Ball and the Deformation of the Ring Net Obtained from the LS-DYNA Simulation; and (Left) The Actual Experiment by Volkwein (2004)**

A.6   References

Arup (2013). *Pilot Numerical Investigation of the Interactions between Landslide Debris and Flexible Debris-Resisting Barriers, Interim Report No. 1.* Report prepared for Geotechnical Engineering Office, Hong Kong, 70 p.

Grassl, H.G. (2002). *Experimentelle und numerische Modellierung des dynamischen Frag- und Vergormungsverhaltens von hochflexiblen Schutzsystemen gegen Steinschlag.* PhD Thesis, Technical Sciences of the Swiss Federal Institute of Technology Zurich, 156 p. (in German)

Volkwein, A. (2004). *Numerical Simulation of Flexible Rockfall Protection Systems.* PhD Thesis, Swiss Federal Institute of Technology Zürich, Switzerland, 134 p. (in German)

GEO PUBLICATIONS AND ORDERING INFORMATION
土力工程處刊物及訂購資料

A selected list of major GEO publications is given in the next page. An up-to-date full list of GEO publications can be found at the CEDD Website http://www.cedd.gov.hk on the Internet under "Publications". Abstracts for the documents can also be found at the same website. Technical Guidance Notes are published on the CEDD Website from time to time to provide updates to GEO publications prior to their next revision.

部份土力工程處的主要刊物目錄刊載於下頁。而詳盡及最新的土力工程處刊物目錄，則登載於土木工程拓展署的互聯網網頁 http://www.cedd.gov.hk 的"刊物"版面之內。刊物的摘要及更新刊物內容的工程技術指引，亦可在這個網址找到。

Copies of GEO publications (except geological maps and other publications which are free of charge) can be purchased either by:

讀者可採用以下方法購買土力工程處刊物(地質圖及免費刊物除外):

Writing to
Publications Sales Unit,
Information Services Department,
Room 626, 6th Floor,
North Point Government Offices,
333 Java Road, North Point, Hong Kong.

書面訂購
香港北角渣華道333號
北角政府合署6樓626室
政府新聞處
刊物銷售組

or
- Calling the Publications Sales Section of Information Services Department (ISD) at (852) 2537 1910
- Visiting the online Government Bookstore at http:// www.bookstore.gov.hk
- Downloading the order form from the ISD website at http://www.isd.gov.hk and submitting the order online or by fax to (852) 2523 7195
- Placing order with ISD by e-mail at puborder@isd.gov.hk

或
- 致電政府新聞處刊物銷售小組訂購 (電話：(852) 2537 1910)
- 進入網上「政府書店」選購，網址為 http://www.bookstore.gov.hk
- 透過政府新聞處的網站 (http://www.isd.gov.hk) 於網上遞交訂購表格，或將表格傳真至刊物銷售小組 (傳真：(852) 2523 7195)
- 以電郵方式訂購 (電郵地址：puborder@isd.gov.hk)

1:100 000, 1:20 000 and 1:5 000 geological maps can be purchased from:

讀者可於下列地點購買1:100 000、1:20 000及1:5 000地質圖：

Map Publications Centre/HK,
Survey & Mapping Office, Lands Department,
23th Floor, North Point Government Offices,
333 Java Road, North Point, Hong Kong.
Tel: (852) 2231 3187
Fax: (852) 2116 0774

香港北角渣華道333號
北角政府合署23樓
地政總署測繪處
電話: (852) 2231 3187
傳真: (852) 2116 0774

Requests for copies of Geological Survey Sheet Reports and other publications which are free of charge should be directed to:

如欲索取地質調查報告及其他免費刊物，請致函：

For Geological Survey Sheet Reports which are free of charge:
Chief Geotechnical Engineer/Planning,
(Attn: Hong Kong Geological Survey Section)
Geotechnical Engineering Office,
Civil Engineering and Development Department,
Civil Engineering and Development Building,
101 Princess Margaret Road,
Homantin, Kowloon, Hong Kong.
Tel: (852) 2762 5380
Fax: (852) 2714 0247
E-mail: jsewell@cedd.gov.hk

免費地質調查報告:
香港九龍何文田公主道101號
土木工程拓展署大樓
土木工程拓展署
土力工程處
規劃部總土力工程師
(請交:香港地質調查組)
電話: (852) 2762 5380
傳真: (852) 2714 0247
電子郵件: jsewell@cedd.gov.hk

For other publications which are free of charge:
Chief Geotechnical Engineer/Standards and Testing,
Geotechnical Engineering Office,
Civil Engineering and Development Department,
Civil Engineering and Development Building,
101 Princess Margaret Road,
Homantin, Kowloon, Hong Kong.
Tel: (852) 2762 5346
Fax: (852) 2714 0275
E-mail: florenceko@cedd.gov.hk

其他免費刊物:
香港九龍何文田公主道101號
土木工程拓展署大樓
土木工程拓展署
土力工程處
標準及測試部總土力工程師
電話: (852) 2762 5346
傳真: (852) 2714 0275
電子郵件: florenceko@cedd.gov.hk

MAJOR GEOTECHNICAL ENGINEERING OFFICE PUBLICATIONS
土力工程處之主要刊物

GEOTECHNICAL MANUALS

Geotechnical Manual for Slopes, 2nd Edition (1984), 302 p. (English Version), (Reprinted, 2011).

斜坡岩土工程手冊(1998)，308頁(1984年英文版的中文譯本)。

Highway Slope Manual (2000), 114 p.

GEOGUIDES

Geoguide 1	Guide to Retaining Wall Design, 2nd Edition (1993), 258 p. (Reprinted, 2007).
Geoguide 2	Guide to Site Investigation (1987), 359 p. (Reprinted, 2000).
Geoguide 3	Guide to Rock and Soil Descriptions (1988), 186 p. (Reprinted, 2000).
Geoguide 4	Guide to Cavern Engineering (1992), 148 p. (Reprinted, 1998).
Geoguide 5	Guide to Slope Maintenance, 3rd Edition (2003), 132 p. (English Version).
岩土指南第五冊	斜坡維修指南，第三版(2003)，120頁(中文版)。
Geoguide 6	Guide to Reinforced Fill Structure and Slope Design (2002), 236 p.
Geoguide 7	Guide to Soil Nail Design and Construction (2008), 97 p.

GEOSPECS

Geospec 1	Model Specification for Prestressed Ground Anchors, 2nd Edition (1989), 164 p. (Reprinted, 1997).
Geospec 3	Model Specification for Soil Testing (2001), 340 p.

GEO PUBLICATIONS

GCO Publication No. 1/90	Review of Design Methods for Excavations (1990), 187 p. (Reprinted, 2002).
GEO Publication No. 1/93	Review of Granular and Geotextile Filters (1993), 141 p.
GEO Publication No. 1/2006	Foundation Design and Construction (2006), 376 p.
GEO Publication No. 1/2007	Engineering Geological Practice in Hong Kong (2007), 278 p.
GEO Publication No. 1/2009	Prescriptive Measures for Man-Made Slopes and Retaining Walls (2009), 76 p.
GEO Publication No. 1/2011	Technical Guidelines on Landscape Treatment for Slopes (2011), 217 p.

GEOLOGICAL PUBLICATIONS

The Quaternary Geology of Hong Kong, by J.A. Fyfe, R. Shaw, S.D.G. Campbell, K.W. Lai & P.A. Kirk (2000), 210 p. plus 6 maps.

The Pre-Quaternary Geology of Hong Kong, by R.J. Sewell, S.D.G. Campbell, C.J.N. Fletcher, K.W. Lai & P.A. Kirk (2000), 181 p. plus 4 maps.

TECHNICAL GUIDANCE NOTES

TGN 1	Technical Guidance Documents